國 立 交 通 大 學

電子工程學系 電子研究所碩士班

碩 士 論 文

高靈敏度之堆疊式結構矽鍺奈米線於不同氧化條件下之氧化特性研究

The Study of Oxidation Characteristics of High Sensitivity Stacked SiGe/Si-On-Insulator Nanowire under Different Oxidation Conditions

研 究 生：吳金濘

指導教授：張國明 教授

中 華 民 國 一〇〇 年 八 月

高靈敏度之堆疊式結構矽鍺奈米線於不同氧化條件下之氧化特性研究

The Study of Oxidation Characteristics of High Sensitivity Stacked SiGe/Si-On-Insulator Nanowire under Different Oxidation Conditions

研究生:吳金濘　　Student : Chin-Ning Wu

指導教授:張國明博士　　Advisor : Dr.Kow-Ming Chang

國 立 交 通 大 學

電子工程學系　電子研究所碩士班

碩士論文

A Thesis

Submitted to Department of Electronics Engineering & Institute of Electronics College of Electrical and Computer Engineering

National Chiao Tung University

in partial Fulfillment of the Requirements

for the Degree of

Master

in

Industrial Technology R & D Master Program on

Microelectronics and Nano Sciences

August 2011

Hsinchu, Taiwan, Republic of China

中 華 民 國 一〇〇 年 八 月

高靈敏度之堆疊式結構矽鍺奈米線於不同氧化條件下之

氧化特性研究

學生：吳金濘　　指導教授：張國明 教授

國立交通大學

電子工程學系　電子研究所碩士班

摘　要

矽奈米線在生物感測上的應用在近幾年已被廣泛的研究及探討，且被視為最具潛力的元件之一。本實驗室團隊成功的製作出矽鍺奈米線，並證實了矽鍺奈米線亦具有與矽奈米線相同的感測特性。本論文中，利用半導體製程技術製作出不同厚度的堆疊式結構和不同矽鍺濃度比的 P 型矽鍺奈米線於 spacer 上。接著進行氧化處理，使鍺從矽鍺奈米線中析出於表面，使原來為均質的矽鍺奈米線變成非均質的矽鍺奈米線，再藉由改變氧化時所通入氧氣及氮氣的比例以及氧化時間。最後，找出最佳的矽鍺濃度比、氮氧比以及氧化時間，使矽鍺奈米線表面與欲感測物產生最好鍵結，以提高靈敏度。

The study of oxidation characteristics of high sensitivity stacked SiGe/Si-on-insulator nanowire under different oxidation conditions

Student: Chin-Ning Wu Advisor: Dr. Kow-Ming Chang

National Chiao Tung University

Department of Electronics Engineering & Institute of Electronics

ABSTRACT

Recently, silicon nanowires (SiNWs) have been extensively studied and discussed in bio-sensor applications, and considered as one of the most promising candidate for sensor devices. We successfully fabricated silicon germanium nanowires (SiGeNWs), and confirmed that it has the same characteristics as SiNWs. In this thesis, the P-type SiGeNWs on the sidewall spacer be fabricated by stacked structure of different thickness and different silicon germanium concentration. Followed by oxidation, we change the oxygen/nitrogen ratio and oxidation time, then observed the Ge will condensation on the surface from SiGeNWs, so that the homogeneous SiGeNWs will become a non-homogeneous SiGeNWs. Finally, find the best concentration ratio of silicon germanium, the nitrogen/oxygen ratio, and the oxidation time, so that the surface of SiGeNWs with some we want to sense to produce the best bonding to improve sensitivity.

誌 謝

首先要感謝 張國明教授在這兩年中的指導，讓我在學業上能有所精進，不僅如此，老師也常常分享自己在求學經過所遇到的問題以及生活上的經驗，尤其是在道德倫理方面我們學到了很多做人、處事的道理，所以很感謝老師用心的教導。

其次要感謝的是實驗室的學長、同學、學弟們與指導或協助我完成論文及實驗的陳巨峰學長、王育彬學長、劉重顯學長、謝政廷同學，很感謝你們在實驗上的指導，讓我在研究論文時可以學到很多的專業知識。另外要特別感謝同屆的同學們及學弟們，因為有你們的鼓勵以及幫助，讓我在做實驗的時候得以解決許多問題，最後能順利完成論文。

此外要感謝國家奈米元件實驗室(NDL)與交通大學奈米中心(NCTU - NFC)提供良好的實驗環境使我順利完成研究，並感謝所有的工程師、技術員以及客服人員們，因為有你們的幫忙，才能使我的研究順利。

最後要感謝的是我的家人，因為有你們的支持以及體諒，我才能全心全力的放在學業上，並且順利的完成學業，謝謝你們。

Content

Figure Captions

Chapter 1

Introduction

1.1 Overview of nanowire sensors

Today, we know that a planar field effect transistor (FET) can be configured as a sensor by modifying the gate oxide is not that using gate electrode, but that with molecular receptors or a selective membrane for the analyte of interest; binding with a charged species, then the major carriers will depletion or accumulation with-in the transistor structure [1, 2]. An attractive feature of such a chemical-sensitive FET is binding that can be a monitor by changing the conductance or related electrical properties [3].

But on the other hand, the small size of nanowire (NW) has more advantage than the planar FET. For example, NW is the large surface-to-volume ratio, which is crucial for ultrasensitive detection of chemical or biological species, and increase sensitivity to the point that single-molecule detection is possible. Physical properties of NW are greatly influenced by surface adsorption of chemical species or bio-molecules, and the adsorption event can be transduced into processable signal, electrical or optical signal. Then these signals can be applied on sensor and detector such as pH sensor, DNA sensor, protein

detection, virus detection and gas detection.

In view of the above-mentioned, more and more researches focus on NW-based sensors in field effect transistor (FET), in which has a single NW or NW array that bridged between source and drain. Nanowire FET sensor enables label-free and real-time detection, direct electrical readout and high device packing density. Further, various kinds of NWs are utilized to fabricate NW-based chemical sensors, including semiconducting metal-oxide NWs, metal NWs, conducting polymer NWs, carbon nanotube (NT), and silicon NW (SiNW).

Among these, carbon NT and SiNW are the most promising candidates for bio-sensing applications. NTs have some good properties, but at the same time also limited in their development. First, during mixed produce of metallic and semiconducting NTs, which make systematic studies difficult because metallic “devices” will not function as expected. Second, flexible methods for the modification of NT surfaces, which are required to prepare interfaces selective for binding a wide range of analytes, are not well established [3].

1.2 Silicon nanowire fabrication

Most of the SiNWs fabrication processes utilize bottom-up approach and top-down approach.

1.2.1 Bottom-up approaches of SiNW fabrication

Bottom-up means that nanostructures are naturally formed on substrate under certain conditions. On the other hand, the NW fabrication (on another wafer) processes utilize nonlithographic methods that will be grew in random, such as thermal evaporation, laser ablation, and Vapor-Liquid-Solid (VLS). Thus need complicated techniques, e.g., fluidic flow [4], showed in Fig.1-1, electric- or magnetic-field directed schemes [4, 5], showed in Fig.1-2, and "pick-and-place" with Atomic Force Microscope (AFM) tip [6], showed in Fig.1-3, to arrange wires for achieving specific functionality [7].

Thermal evaporation technique, mixture of Si and SiO_2 [8] or SiO [9] only is presented as a way of SiNW fabrication. In this paper mentioned that SiNWs obtained by thermal evaporation are covered by SiO_2. In addition, the substrate temperature is shown to be crucial for diameter control and NW morphology by Peng and co-workers [10]. In general, SiNWs synthesized by thermal evaporation latent some problems, such as high defect density and oxygen incorporation.

Then laser ablation technique with high purity and high yields SiNW synthesis was reported by Zhang and co-workers. The crystalline NWs with diameters ranging from 3 to 43nm and lengths up to a few hundred microns were synthesized in their study [11]. Furthermore, adding SiO_2 into Si target enhanced the growth of silicon synthesized by laser ablation, and SiO_2 was more important than metal in catalyzing the NW formation

[12].

Vapor-Liquid-Solid (VLS) technique is one of the most common approaches for SiNW fabrication. In VLS process, metal nanoclusters that form low temperature eutectic phase with silicon are dispersed on substrate and serve as the catalyst for SiNW growth. The catalyst, liquid droplet, is a preferred site for deposition from the vapor that is compound of Si, such as SiI_2 or $SiCl_4$. There are three important facts followed: (a) silicon whiskers have no axial screw dislocation; (b) an impurity is essential; [13] (c) a small globule is remained at the tip of the NW. The fact (a) mechanism was confirmed by the Frank [14]. And the facts (b) and (c) mechanism, the impure role is to form a liquid alloy droplet of relatively low freezing temperature [15], showed in Fig.1-4.

1.2.2 Top-down approaches of SiNW fabrication

Generally, most of top-down approaches are based on lithography, such as electron beam lithography (EBL), EUV or ion beam lithography, which is high cost facilities. In fact, top-down approaches are most of the VLSI techniques belong to this category because it greatly facilitates system integration in large scale. In order to improve economic limitations and bad-controlled NWs, top-down approaches need some manners for low-cost, such as nanoimprint lithography [16], ashing-trimming technology [17] and spacer patterning [18].

Ashing-trimming technique is combined with resist ashing and oxide hard mask trimming. These techniques require neither specific equipment

nor materials to achieve that the line width beyond the limit of optical lithography or high-throughput-beam lithography. Because this technology improve the width of photoresist to narrower in ashing process, and then improve the width of oxide to narrower in trimming process.

Spacer patterning technology using the residuum, sidewall spacer, takes as hard mask in plasma etching process. Choi and co-workers demonstrated to achieve sub-7 nm structures with conventional dry etching. And in this paper mentioned that the yield of critical dimension (CD) variations of minimum-sized features much smaller than that achieved by optical or EBL. Not only that, it also provides a doubling of device density for a given lithography pitch, showed in Fig.1-5 [18].

NWs with the size are beyond the limit of lithography, some techniques are developed to further reduce the size of NWs after wires are formed, including oxidation, electrochemical etching [19] and anisotropic wet etching [20]. Electrochemical approach is presented by Robert Juhasz and co-workers [19]. It offers three operation regimes: polishing, macropore formation, and porous formation, and successfully fabricated SiNW with 9nm diameter and very smooth surface by setting appropriate etching parameters. Fig. 1-6 shows the optical images of chip layout and schematic cross-section of the etching setup. Besides, anisotropic wet etching is proposed by E. Stern and his co-workers [20]. It is highly controllable and reproducible, and mobility degradation is prevented. Because of Tetramethylammonium hydroxide (TMAH) is used to etch pre-fabricated wires into nanoscale. Fig. 1-7(a) shows the schematic

diagram of a nanowire device after anisotropic etching, and Fig. 1-7(b) is the SEM image of a nanowire device.

In fact, a single NW channel is restricted by current drivability about a few microamperes, which could be a limiting factor for applications like analog and RF. So some group successfully built more NWs per device to increase the drive current, such as horizontally SiNW array channel [21] and vertically stacked array channel CMOS transistor [7, 22]. However, the former arraying alone impacts the density of integration, and the lateral is expected to address this issue to a large extent.

1.3 Applications of SiNW sensors

SiNWs have been extensively studied and discussed in bio-sensor applications, such as pH sensor, DNA sensor, protein detection, virus detection, and gas detection. They apply on that we want to sense will binding with the surface of SiNW, so that conduction of SiNW changed. And the detail is followed.

1.3.1 pH sensor

SiNW applied to pH sensors [3, 22]. Lieber's group [3] researched the response of SiNWs with and without 3-aminopropyltriethoxysilane (APTES) surface modification. The device structure and the response are shown in Fig. 1-8, unmodified SiNWs showed nonlinear response, and APTES-modified exhibited linear pH dependence. SiNWs' surface have

APTES-modified and unmodified, and then the surface terminating in both $–NH_2$ and –SiOH groups which have different dissociation constants. In other words, the surface of APTES-modified SiNW has $–NH_2$ group was protonated to $–NH_3^+$at low pH. On the contrary, the surface of unmodified SiNW has –SiOH group was not easy to protonated to $–SiOH_2^–$.

1.3.2 DNA sensor

DNA detection is a very important area in biological science and technology. For example, Hahm and co-workers [23] have reported p-type SiNWs apply on peptide nucleic acid (PNA) receptors function as ultrasensitive and selective real-time DNA sensors at concentrations down to tens of femtomolar range. Besides, Li and co-workers [24] demonstrated a highly sensitive and sequence-specific DNA sensor that the surface of SiNWs can covalent with single stranded (ss) DNA probes. In addition, Gao and co-workers [25] demonstrated PNA functionalized SiNW arrays were capable of detecting complementary target DNA, as shown in Fig.1-9 and the resistance change was concentration-dependent, shown in Fig.1-10.

1.3.3 Protein detection

In fact, Lieber's group researched not only on pH sensors but also on protein detection [3]. And they are the first demonstration of label-free

electronic detection of biological and chemical species in solution using SiNW FET. Fig. 1-11 (A) illustrated biotin-modified SiNW surface was bond by streptavidin before and after, and Fig. 1-11 (B) shows the conductance change corresponding to streptavidin detection. In this paper, the conductance of biotin-modified p-type SiNW sensors increased when solutions of streptavidin protein were delivered into microfluidic channel, binding between biotin and streptavidin, which bond was strongly even after the addition of pure buffer solution.

Recently, the same group reported multiplexed, real-time, and label-free detection of cancer marker proteins, down to femtomolar concentrations, in a single platform [26]. SiNWs were aligned over a large area at the center of the chip by fluid-based assembly and formed more than 100 independently and electrically addressable arrays, which facilitate multiplexed detection. Fig. 1-12 shows the optical image of NW device arrays. Antibodies-modified SiNW sensors exhibited complementary response from p-type and n-type NWs (Fig. 1-13, the result of the conductance changed was just the opposite), and highly selective detection of prostate-specific antigen (PSA), bovine serum albumin (BSA), and mucin-1 simultaneously, as shown in Fig. 1-14.

1.3.4 Virus detection

Viruses are one of the most important causes of human disease. And the virus sensors based on NW-FET presented by Patolsky and co-workers [27]. In this paper, they have been reported direct, real-time

electrical detection of single virus particles with high selectivity by using NW-FET that was modified with different antibody receptors, as shown in Fig. 1-15. On the other hand, they has been demonstrated for only two distinct viruses in this work, but assembly methods have demonstrated much larger arrays of reproducible NW devices [28] that might simultaneously screen for the presence of 100 or more different viruses.

1.3.5 Gas detection

Gas detection is very important for some dangerous gases, such as H_2, and $POCl_3$. In addition, detecting leak gas which is an important case, it can cost-saving. For example, Wan and co–workers [29] have demonstrated a novel SU8/SiO_2/PMMA trilayer nanoimprint technique to fabricate the p-type SiNWs sensor detected gas, NO_2 and NH_3, as shown in Fig. 1-16. The response of NO_2 was

$$NO_2 + e^- \rightarrow NO_2 \qquad \text{(eq.1.1)}$$

Then the p-type SiNWs was accumulation, such that the conductance increasing. On the other hand, the response of NH_3 was

$$NH_3 + H^+ \rightarrow NH_4^+ \qquad \text{(eq.1.2)}$$

Then the p-type SiNWs was depletion, such that the conductance decreasing.

1.4 Other materials of nanowire sensors

Actually, many groups researched sensors of non-Si based, such as

metal oxide semiconductor nanowire sensor, and metal nanowire sensor. And the detail is followed.

1.4.1 Metal oxide nanowire sensor

Some groups successfully demonstrated chemical sensors based on semiconducting metal oxide 1D nanostructures, including nanotube [30], nanobelt [31], nanorod [32], nanoribbon [33], and nanowire. Various kinds of metal oxide wire-like nanostructures were reported, including ZnO, In_2O_3, SnO_2, Co_3O_4, Fe_2O_3, TiO_2, MoO_3, and V_2O_5. Among these, most attention had been focused on SnO_2, ZnO, and In_2O_3.

Moskovits and co-workers [34] investigated the O_2 and CO sensing properties of SnO_2 NW sensors and concluded that exposure to O_2 created the surface acceptor states such that reduced the conductance. On the contrary, exposure to combustible gases like CO led to oxidation-reduction reaction at the surface and reduced the surface oxygen concentration, increasing the conductance eventually. Afterward, they studied the interaction between surface reactivity and the electron density inside the nanowire, which is related to gate voltage [35]. And they confirmed that the rate and extent of oxygen ionosorption and CO oxidation reaction are controllable by applying different gate voltages [36].

ZnO nanostructures in the form of nanorod, nanotube, and nanowire are reported, which exhibit very high surface-to-volume ratio. Safaa and co-workers [32] developed ZnO nanorods to be pH sensor. They reported

ZnO nanorods grown on two-dimensional macroporous periodic structures (2DMPPS) *n*-Si substrate as compared to plane *n*-Si at room temperature. And the *p*H sensing range was from 4 to 12 in buffer and NaCl solutions.

At last, the series of studies on In_2O_3 NW sensors was reported by Zhou's group [37]. They used individual In_2O_3 nanowire transistors as chemical sensors working at room temperature. When NW transistors exposure to a small amount of NO_2 or NH_3, the conductance will decrease (up to six or five orders of magnitude, as shown in Fig.1-17) and also substantial shifts in the threshold voltage, as shown in Fig.1-18. The response times were 5sec for 100-ppm NO_2 and 10sec for 1% NH_3, and the lowest detectable concentrations are 0.5 ppm for NO_2 and 0.02% for NH_3. Continuously, they pushed the detection limit of NO_2 to 5ppb by using multiwire nanowire sensors [38] and attributed this improvement to the nanowire/nanowire junctions between metal electrodes.

1.4.2 Metal nanowire sensor

Many groups successfully fabricated different kind of metal NWs with proper plating solution, electrodeposition parameters, and the help of template. In this, NWs usually were made by ferromagnetic materials. Thus, the NWs are magnetized, and the magnetic dipole lies along the wire's axis, which magnetic nanowires are orientable by applying magnetic field [39]. Similarly, electric field is capable of polarizing and

aligning NWs. Peter and co-workers [40] demonstrated electric field-assisted assembly of Au NWs.

Penner and co-workers [41] fabricated hydrogen sensors based on Pd nanowire array. Fig.1-19 (A) and (B) show the schematic diagram of a palladium mesowire array (PMA) and the SEM image. And Pd mesowires provides a new mechanism by which mesowires can operate as chemical sensors. In other words, it is attributed to the conductivity increase based on hydrogen incorporation and microstructure change. AFM images of Pd nanowire before and after exposure to hydrogen gas are also shown in Fig. 1-19.

The other group, Tao and co-workers [42] fabricated Cu NW arrays to detect 2, 2'-bipyridine (22BPy), adenine, and mercaptopropionic acid (MPA), and studied changes in the quantized conductance of the NWs upon different surface scattering behavior and adsorbates-nanowire interactions.

In addition, Wang and Ozkan [43] reported a p-type heterojunction NW, CdTe-Au-CdTe (semiconductor-metal-semiconductor), to be different DNA sensor with a FET configuration, which was ultrasensitive to detect biomolecules based on the modulation of NW conductance. By the way, on the surface it is more sensitive compare to metallic NW. In addition, the Au segment benefits sensor performance by good functionalization capability of DNA binding, as shown in Fig.1-20.

1.5 Sensitivity

Sensitivity of NW-based sensor is defined as the ratio of conductance change, caused by the surface of NW binding before and after. NW-based sensors exhibit higher sensitivity than planar sensors, because the surface-to-volume ratio is larger. And Fig.1-21 [44] shows the simulated conductance values of SiNW as a function of the surface potential consider the different width. Obviously, the smaller width is more sensitive to surface potential.

In addition to scaling, there is some method can improve sensitivity followed: 1) choosing non-Si-based NW, such as metal nanowire or SiGe nanowire, 2) surface engineering, which is Au-nanoparticle-modified SiNW reported by Kun [45], because Au can provide better binding to thiol group at the surface, 3) structure engineering, such as heterojunction CdTe-Au-CdTe nanowire proposed by Wang [43].

In this thesis, we focus on semiconductor nanowires, such as Si and SiGe nanowires. Here, we assume them as an ideal cylindrical semiconducting channel in macro-scale with diameter d, length L_{NW}, doping density N_D, we can easily derive a simplified expression of conductance, conductance variation, and sensitivity respectively as follows [46]

$$G_0 = \frac{q\mu N_D \pi d^2}{4L_{NW}} \qquad \text{(eq1.3)}$$

$$\Delta G = \frac{\pi d \mu \sigma}{L_{NW}} \qquad \text{(eq1.4)}$$

$$S = \frac{|\Delta G|}{G} = \frac{4\sigma}{qdN_D} \qquad \text{(eq1.5)}$$

, where q is 1.6 x10^{-19}C, μ is carrier mobility, σ is surface charge density.

1.6 Ge condensation technology

This phenomenon is one of the most important for our investigated. As fabricating SiNW, we always want to the nanowire size can be reduced. There are three ways to reduce nanowire size, include oxidation, anisotropic wet etching, and electrochemical method. Now, if we do oxidation for SiGe, Ge would condensation (on the interface between SiGe and SiO_2) from SiGe. Because of that, oxidation of SiGe is also named Ge condensation. This phenomenon is observed in 1980s [47] and receives a lot of attention since then owing to the importance of SiGe and Ge for electronic and optoelectronic devices [48].

According to the ternary phase diagram of Si-Ge-O system at 1000K, which is shown in Fig. 1-22 [49], it tell us that as long as pure Si exists, no GeO_2 is formed under equilibrium condition. Because of that when GeO_2 is in contact with Si_xGe_{1-x}, GeO_2 will be reduced, according to the reaction

$$Si+GeO_2 \rightarrow SiO_2+Ge. \qquad \text{(eq.1.6)}$$

And Ge is completely rejected from SiO_2 and piles up at SiO_2/SiGe interface, as shown in Fig.1-23 [50]. The thickness of this Ge-rich region at interface depends on oxidation temperature and duration, which determine the Ge diffusion behavior. Besides, the effect of oxidation

temperature and annealing are studied by several groups, aiming at obtaining high quality and high Ge concentration SiGe film. It's demonstrated that defect free and strain relaxed Ge-rich SiGe film can be obtained.

In recent years, Ge condensation technology is applied on fabricating silicon germanium on insulator (SGOI) and even germanium on insulator (GOI). SGOI not only provides the same advantages as SOI, but also SiGe layer can serve as channel material or induce strain to Si channel, which can increase the carrier mobility and improve device performance.

In our study, we utilize this technology to reduce NW size and at th same time the Ge concentration is rise, which greatly enhances sensitivity.

Chapter 2

Experiment

For our group investigation, SiGe and Si nanowires were fabricated by top-down approach. We used spacer formation to obtain SiGe and Si spacers on nanometer scale as SiGe and Si nanowires. And we used Ge condensation technique to increase the Ge concentration and reduce the NW size.

2.1 Process flow

First, we started with p-type (Boron doped) Si substrate (100), and the resistivity was 1.5-100Ω・cm. And then the process followed:

1. Standard RCA cleaning.
2. 6 hrs 40min wet oxidation at 980℃ to grow 5000 Å by ***SVCS Furnace system***, shown in Fig.2-1.
3. ***TEL CLEAN TRACK MK-8*** and ***Canon FPA – 3000i5+ stepper lithography system*** were employed to transfer the pattern of Mask #1 to oxide layer.
4. Dry etching was carried out with ***TEL 5000 R.I.E. system*** to form oxide step for 3000 Å depth, the structure is shown in Fig. 2-2.
5. Standard RCA clean.
6. About 3hrs deposition α-Si layer for 200 Å and 400 Å at 650℃ by

SVCS Furnace system.(This step served as seed layer for SiGe film.) The structure is shown in Fig. 2-3.

7. Standard RCA clean.
8. At 665℃, SiGe deposition by ***ANELAVA SiGe UHV-CME***, and poly Si deposition by ***SVCS Furnace system***. The structure is shown in Fig. 2-4.
9. Patterning the pattern of Mask #2.
10. Poly Si and SiGe dry etching was carried out with ***TCP9400 SE*** poly etcher to remove unwanted part. Defined the S/D region and SiGe or Si nanowires on the sidewall spacer. The structure is shown in Fig. 2-5.
11. Patterning the pattern of Mask #3.
12. Using ***TCP 9400 SE*** poly etcher to remove unwanted sidewall spacer, which would result short circuit between two nanowire devices if not removed. The structure is shown in Fig. 2-6.
13. Boron-fluoride (BF_2) ion implantation by ***Implantation E500HP***. The implantation dose is 1×10^{15} ions/cm^2, and the implantation energy was 50keV. The structure is shown in Fig. 2-7.
14. Annealing in furnace at 950℃ for 30min to activate carriers.
15. 5000Å Aluminum deposition by ***AST Peva 600I***. The structure is shown in Fig. 2-8.
16. Defined contact pad by Mask #4.
17. Etching Al pads, and defining the contact by wet etching (HNO3:CH3COOH:H3PO4:H2O=2:9:50:10). The structure is shown in Fig. 2-9.

18.Al sintering at 400℃ in N_2 ambient for 30 minutes.

2.2 Functionalization

At first, we used 3-Aminopropyl-trimethoxysilane (APTMS) to modify the surface of native oxide layer around nanowires, as shown in Fig.2-10. When we dripped the APTMS down to the surface of native oxide layer, the hydroxyl functional groups were replaced by the methoxy groups of APTMS molecule. And the terminal of APTMS groups was amine groups, which were prone to be positively charge; it is similar that FET give a positive bias, so that the conductance of p-type nanowires decreased. The next, we used Bis-sulfosuccinimidyl-suberate to bond with APTMS. In addition, BS3 treatment resulted in negative charge, thus the conductance increased.

2.3 Measurement of electric characteristics

We measured the electric characteristics of nanowire sensors by HP4156A. Giving the drain voltage (V_D) was varied from -10V to 10V, the step voltage was 100mV, and the back gate voltage (V_g) was 0V. The electric measurement of electric characteristics was performed at every stage of surface modification, and the average conductance was then extracted from I_D-V_D characteristics with V_D=4~6V.

2.4 Calculation of sensitivity

First, we measured *I-V* curve for no treatment devices, and then we set the current as I_0. Second, we dripped the APTMS to the surface of SiGe nanowires, and the measured *I-V* curve. Then we set the current as I. And the sensitivity was

$$S = \frac{|I - I_0|}{I_0} \qquad \text{(eq.2.1)}$$

Chapter 3

Results and Discussion

3.1 Motive of the experiment

We covered the surface of SiNW with SiGe to increase sensitivity in our group's previous research. The concentration of Ge would be raised by oxidation, and we could find better quality of deposited SiGe layer, and then the high density of Ge would be separated on surface, which is non-homogeneous structure. Besides, we can obviously realize that Ge only remains on the surface of nanowire by AUGER analysis, and the sensitivity happens to be decreased when the density of Ge increases. We assume that the higher concentration of Ge will increase vacancies on the surface, which will not easy for objects under test to bond and decrease sensitivity. Then we console the characteristic of oxidation of Si, the oxidation process with nitrogen can repair the vacancies of surface and improve the quality of oxide in order to increase sensitivity.

The procedure of the experiment is showed as Fig.3-1. We put nanowires of Poly-Si, $Si_{0.93}Ge_{0.07}$, and $Si_{0.86}Ge_{0.14}$ $Si_{0.80}Ge_{0.20}$ in combination of amorphous Si 200Å and 400Å, and the nitrogen flow for 0%, 13.33%, 20%, 40%, and 100%, and 900℃ to oxidize for 3, 5, 7, 10minutes. But for the ratio of N_2 is 100% has no the procedure of

oxidation for 5, 7, 10minutes. And then we try to find out a best combination in the experiment to increase the sensitivity.

The Fig.3-2 showed the SEM image of Poly-Si nanowire. The structure of 200Å 7%, which means the thickness of amorphous Si was 200Å and the concentration of Ge was 7% in SiGe ($Si_{0.93}Ge_{0.07}$), as shown in Fig.3-3, which showed the width of nanowire was 72.2nm. The structure of 200Å 14% showed in Fig.3-4, which showed the width of nanowire was 77.8nm. The structure of 200Å 20% showed in Fig.3-5, which showed the width of nanowire was 65nm. The structure of 400Å 7% imaged Fig.3-6, which showed the width of nanowire was 67nm. The structure of 400Å 14% imaged Fig.3-7, which showed the width of nanowire was 75.0nm.

3.2 Electrical response after dripping APTMS and BS3

The APTMS and BS3's bond structures contain positive and negative electricity respectively, such as the conductance will decrease after dripping APTMS on p-type nanowire, but it will increase when the bonds of BS3 which drips on APTMS.

For the thickness of amorphous Si was 200Å (α-Si 200Å) and $Si_{0.86}Ge_{0.14}$ in oxidation time was 3min, the flow ratio of N_2 was 13%, and L=11 μm, the variation of current was shown in Fig.3-8 and conductivity was shown in Fig.3-9.

3.3 The sensitivity discussion for three minutes oxidation

3.3.1 The sensitivity discussion in varied stack structure under different nitrogen/oxygen ratio

At the first, we see Fig.3-10, which provide the sensitivity of varied stack structures for 3min oxidation time in different nitrogen/oxygen ratio. We found that for no treatment and N_2 100% (no oxidation), $Si_{0.80}Ge_{0.20}$ has the larger sensitivity for α-Si 200Å , and $Si_{0.86}Ge_{0.14}$ is α-Si 400Å . In addition, the integral sensitivity of N_2 100% is larger than no treatment, so we inferred the N_2 could repair the defect at interface. On the other hand, we also observed that after SiGeNW doing the produce of oxidation, $Si_{0.86}Ge_{0.14}$ would become the greater sensitivity for α-Si 200Å and 400Å . Why the sensitivity of α-Si 200Å $Si_{0.80}Ge_{0.20}$ decayed? Because the concentration of Si smaller than χ_c, making hard to occur the reaction

$$Si+GeO_2 \rightarrow SiO_2+Ge \quad [51]. \qquad \text{(eq.3.1)}$$

Thus Ge was oxidized, the concentration of Ge decayed, the sensitivity decayed.

3.3.2 The sensitivity discussion in varied nitrogen/oxygen ratio under different stack structure

The second, we knew that oxidation can increase the sensitivity by Ge condensation. In fact, oxidation of N_2 0% could make more defect at the interface, and then carriers get more scattering, such that the sensitivity decayed, so in process of oxidation we added some nitrogen to

repair the defect, and try to find out the best nitrogen/oxygen ratio for the highest sensitivity. In the Fig.3-11, we found the N_2 13% has the best sensitivity, except Poly-SiNW. This phenomenon causes that when the nitrogen ratio is higher; the radius of Poly-SiNW will be larger after doing the step of oxidation. Thus the current is dispersion, the sensitivity decay. In addition, during the process of oxidation the nitrogen/oxygen ratio was 13%, we found out that the sensitivity has maximum.

3.3.3 The relationship between conductivity and sensitivity

Conductivity

$$G = \frac{\Delta I}{\Delta V} \qquad \text{(eq.3.2)}$$

Where I is current, V is voltage. Let us seeing Fig.3-12, which is the percentage of change amount of sensitivity $\Delta S = \frac{S - S_0}{S_0}$ (where S_0 is the sensitivity of no treatment), and the percentage of change amount of conductivity $\Delta G = \frac{G - G_0}{G_0}$ (where G_0 is the conductivity of no treatment) for 3min oxidation compare to no treatment. We can found that the sensitivity and conductivity is almost overlapped. Thus, we inferred to the conductivity is directly influence to sensitivity.

3.4 The sensitivity discussion for five minutes oxidation

3.4.1 The sensitivity discussion in varied stack structure

under different nitrogen/oxygen ratio

In this section, let us to see Fig.3-13, it provides the sensitivity of varied stack structures for 5min oxidation time in different nitrogen/oxygen ratio. We observed that after SiGeNW doing the produce of oxidation, $Si_{0.86}Ge_{0.14}$ would become the greater sensitivity for α-Si 200Å and 400Å. It is because the concentration of Si smaller than χ_c, making hard to occur the reaction

$$Si+GeO_2 \rightarrow SiO_2+Ge \text{ [51].} \qquad \text{(eq.3.2)}$$

Thus Ge was oxidized, the concentration of Ge decayed, the sensitivity decayed. This result is similar to 3min. On the other hand, we also found that the overall sensitivity of 5min is smaller than 3min. The phenomenon detail is discussed in section 3.6.

3.4.2 The sensitivity discussion in varied nitrogen/oxygen ratio under different stack structure

In fact, we knew that oxidation can increase the sensitivity by Ge condensation. However, oxidation of N_2 0% could make more defect at the interface, and then carriers get more scattering, such that the sensitivity decayed, so in the process of oxidation we added some nitrogen to repair the defect, and try to find out the best nitrogen/oxygen ratio for the highest sensitivity. In the Fig.3-14, we found the N_2 13% has the best sensitivity, except Poly-SiNW. This phenomenon causes that

when the nitrogen ratio is higher; the radius of Poly-SiNW will be larger in the step of oxidation. Thus the current is dispersion, the sensitivity decay. On the other hand, during the process of oxidation the nitrogen/oxygen ratio was 13%, we found out that the sensitivity has maximum. This result is similar to 3min. Besides, we also found that the overall sensitivity of 5min is smaller than 3min. The phenomenon detail is discussed in section 3.6.

3.5 The sensitivity discussion for ten minutes oxidation

3.5.1 The sensitivity discussion in varied stack structure under different nitrogen/oxygen ratio

In this section, let us to see Fig.3-15, it provides the sensitivity of varied stack structures for 10min oxidation time in different nitrogen/oxygen ratio. We observed that after SiGeNW doing the produce of oxidation, $Si_{0.86}Ge_{0.14}$ would become the greater sensitivity for α-Si 200Å , but for α-Si 400Å was $Si_{0.93}Ge_{0.07}$.

The radius of SiGeNWs has smaller for α-Si 400Å than α-Si 200Å , as shown in Fig.3-16, so α-Si 400Å SiGeNW has smaller volume. We inferred that in the process of oxidation, the Ge concentration of α-Si 400Å $Si_{0.86}Ge_{0.14}$ increases faster than α-Si 200Å $Si_{0.86}Ge_{0.14}$. Thus α-Si 400Å $Si_{0.86}Ge_{0.14}$ during 10min oxidation, the concentration of Si already smaller than χ_c, but α-Si 200Å $Si_{0.86}Ge_{0.14}$ not yet. The α-Si 400Å

$Si_{0.86}Ge_{0.14}$ has the same situation as α-Si 200Å was $Si_{0.80}Ge_{0.20}$. That is to say SiGeNWs are hard to occur the reaction

$$Si+GeO_2 \rightarrow SiO_2+Ge \quad [51]. \qquad \text{(eq.3.3)}$$

Thus Ge was oxidized, the concentration of Ge decayed, the sensitivity decayed.

On the other hand, α-Si 200Å for different Ge concentration, the overall sensitivity of 10min is smaller than 5min. The phenomenon detail is discussed in section 3.6.

3.5.2 The sensitivity discussion in varied nitrogen/oxygen ratio under different stack structure

In this section, we knew that oxidation can increase the sensitivity by Ge condensation. However, oxidation of N_2 0% could make more defect at the interface due to no nitrogen to repair defect, and then carriers get more scattering, such that the sensitivity decayed, so in the process of oxidation we added some nitrogen to repair the defect, and try to find out the best nitrogen/oxygen ratio for the highest sensitivity. In the Fig.3-17, we found the N_2 13% still has the best sensitivity, except Poly-SiNW. This phenomenon causes that when the nitrogen ratio is higher; the radius of Poly-SiNW will be larger in the step of oxidation. Thus the current is dispersion, the sensitivity decay. On the other hand, during the process of oxidation the nitrogen/oxygen ratio was 13%, we found out that the sensitivity has maximum. Besides, we also found that the overall sensitivity of 10min is smaller than 5min. The phenomenon

detail is discussed in section 3.6.

In Fig.3-17, it is obvious that after the process of oxidation, the sensitivity is smaller than no treatment due to oxidation time is so long that silicon dioxide grown up slower and slower. Because of above-mentioned, Ge started to diffuse forward to α-Si, thus the current was dispersion, the sensitivity decay.

3.6 The sensitivity discussion in varied oxidation time

3.6.1 The sensitivity discussion in varied oxidation time under 13% nitrogen/oxygen ratio

Base on section 3.3, 3.4, and 3.5, we found out N_2 13% has the highest sensitivity, so we choose N_2 13% to discuss the varied oxidation time.

We have known that during process of oxidation, silicon dioxide could grow up slower and slower. It is because the thick SiO_2 forbidden silicon contact with oxygen. Thus the Ge condensation would be unobvious; opposite the Ge diffusion would dominant. Where the phenomenon of condensation can increase the sensitivity, but phenomenon of diffusion can decrease the sensitivity. Let us to see Fig.3-18, this showed the sensitivity increase with the longer oxidation time for Poly-SiNWs, but for SiGeNWs the sensitivity decrease.

For Poly-SiNWs, this phenomenon causes that when the oxidation

time is longer; the radius of Poly-SiNWs will be smaller in the step of oxidation. Thus the current is centralize, the sensitivity increase. On the other hand, for SiGeNWs, through the oxidation time is longer; the radius of SiGeNWs will be smaller in the step of oxidation, this is not the decisive factor. For SiGeNWs, the oxidation time is too long to Ge diffuse forward to α-Si, and the current was dispersion, the sensitivity decrease.

3.6.2 The sensitivity discussion in varied oxidation time to contrast different stack structure

At first, we focus on α-Si 200Å to contrast on different Ge concentration in varied oxidation time, as shown in Fig.3-19, this say α-Si 200Å $Si_{0.93}Ge_{0.07}$ almost is a linear. Because the SiO_2 grow up become slower during 5min to 10min, the Ge condensation have the same rate for oxidation time from 3min to 5min and 5min to 10min. On the other hand, α-Si 200Å $Si_{0.86}Ge_{0.14}$ and α-Si 200Å $Si_{0.80}Ge_{0.20}$ have the same situation, but the concentration of Ge is too high to the phenomenon of diffusion is the dominant during the oxidation time from 5min to 10min, so it has a steeper slope.

The second, for α-Si 200Å $Si_{0.93}Ge_{0.07}$ and α-Si 400Å $Si_{0.93}Ge_{0.07}$ have the same situation, and the reason as above. Besides, α-Si 200Å $Si_{0.86}Ge_{0.14}$ and α-Si 400Å $Si_{0.86}Ge_{0.14}$ have the same situation; and α-Si 400Å $Si_{0.86}Ge_{0.14}$ is sharper. It is because α-Si 400Å $Si_{0.86}Ge_{0.14}$ not only the above-mentioned but also that the radius of SiGeNWs has smaller for

α-Si 400Å than α-Si 200Å, as shown in Fig.3-16, so α-Si 400Å SiGeNW has smaller volume. Then we inferred that in the process of oxidation, the Ge concentration of α-Si 400Å $Si_{0.86}Ge_{0.14}$ increases faster than α-Si 200Å $Si_{0.86}Ge_{0.14}$. Thus α-Si 400Å $Si_{0.86}Ge_{0.14}$ during 10min oxidation, the concentration of Si already smaller than χ_c, but α-Si 200Å $Si_{0.86}Ge_{0.14}$ not yet. So the sensitivity of α-Si 400Å $Si_{0.86}Ge_{0.14}$ would smaller than no treatment.

Chapter 4

Conclusion

We can summarize the following result according to the data from previous experiment:

1. APTMS generated bond with BS3, and had the electrical response.
2. We successfully fabricated the stack structures, which were α-Si 200Å $Si_{0.93}Ge_{0.07}$, α-Si 200Å $Si_{0.86}Ge_{0.14}$, α-Si 200Å $Si_{0.80}Ge_{0.20}$, α-Si 400Å $Si_{0.93}Ge_{0.07}$, and α-Si 400Å $Si_{0.86}Ge_{0.14}$. All of the several structures had the electrical response, and we found out the structure of α-Si 400Å $Si_{0.86}Ge_{0.14}$ enhanced the highest sensitivity for no treatment.
3. We could increase the density of Ge on the surface of nanowire with the help of oxidation, and sensitivity would increase with the density of Ge.
4. After oxidation, we successfully produced the non-homogeneous structures of SiGe nanowire by Ge condensation, and we confirmed that its sensitivity was better than the homogeneous structure.
5. After oxidation, we found out the structure of α-Si 400Å $Si_{0.86}Ge_{0.14}$ enhanced the highest sensitivity for 3min and 5min oxidation, in addition α-Si 200Å $Si_{0.86}Ge_{0.14}$ enhanced the highest sensitivity for 10min.
6. We compared the N_2 0%, N_2 13%, N_2 20%, N_2 40%. For all stack structure, N_2 13% had more sensitive than the other nitrogen/oxygen ratio.

7. For different oxidation time, 3min enhanced the highest sensitivity.

Chapter 5

Future Works

In my research, we found that the sensitivity of α-Si 200Å $Si_{0.80}Ge_{0.20}$ fall down under 3min oxidation, it was caused by the concentration of Ge was too high to the oxidation rate increase caused more defect. Besides, the sensitivity of α-Si 400Å $Si_{0.86}Ge_{0.14}$ fall down under 10min oxidation, it was caused by the oxidation time too long to the Ge diffuse forward to α-Si cause the current dispersion.

In order to modify above-mentioned, we proposed two ways:

1. We can cap Si on SiGeNWs to modify the high oxidation rate.
2. We can change the temperature during oxidizing to forbid the Ge diffuse.

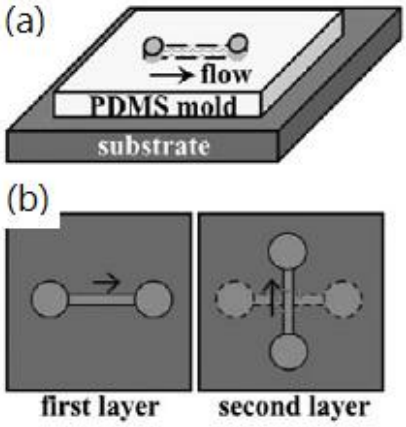

Fig.1-1 Fluidic flow-directed assembly of NWs. Schematic (a) of parallel NW obtained by passing a NW solution through a channel on a substrate; Schematic (b) of crossed NW obtained by orthogonally changing the flow direction in a sequential flow alignment process. Adapted from [52].

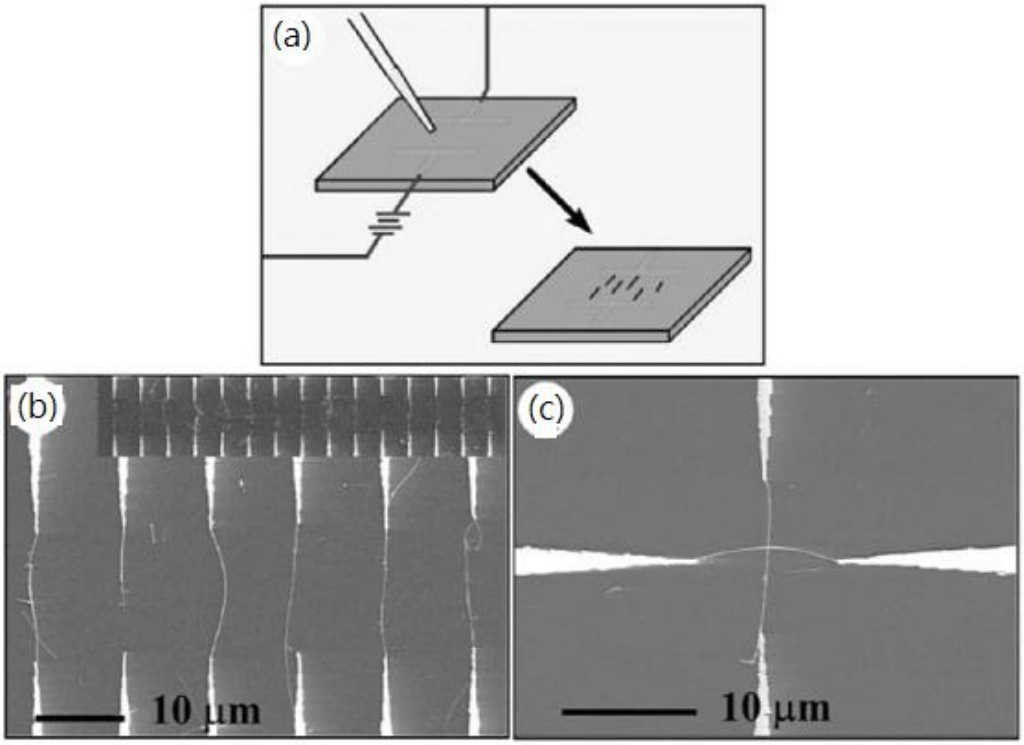

Fig.1-2 Electrical field directed assembly of NWs. Schematic (a) is aligned by E-field. (b) Spatially positioned parallel NWs array obtained

following E-field assembly. The inset of schematic (b) shows 15 pairs of parallel individual NWs bridging between the electrode pair. Schematic (c) shows the crossed NW junction obtained using layer-by-layer alignment with the E-field applied in orthogonal directions. Adapted from [53].

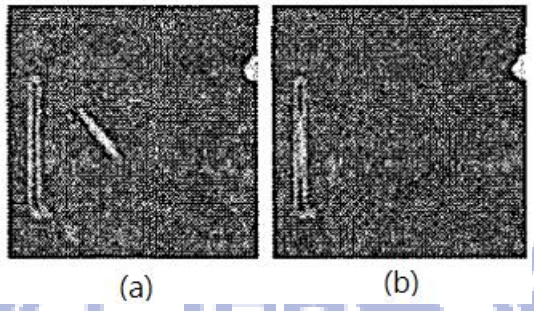

Fig.1-3 The AFM image from (a) to (b) displayed the AFM tip pushing the rod into the fixer. Adapted from [6]

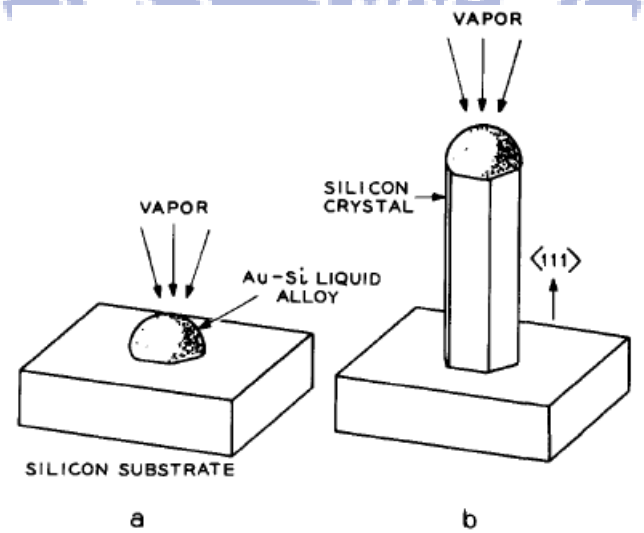

Fig.1-4 Growth of a silicon crystal by VLS. The schematic a. is a liquid droplet on substrate, and the schematic b. is growing crystal with liquid droplet at the tip. Adapted from [15]

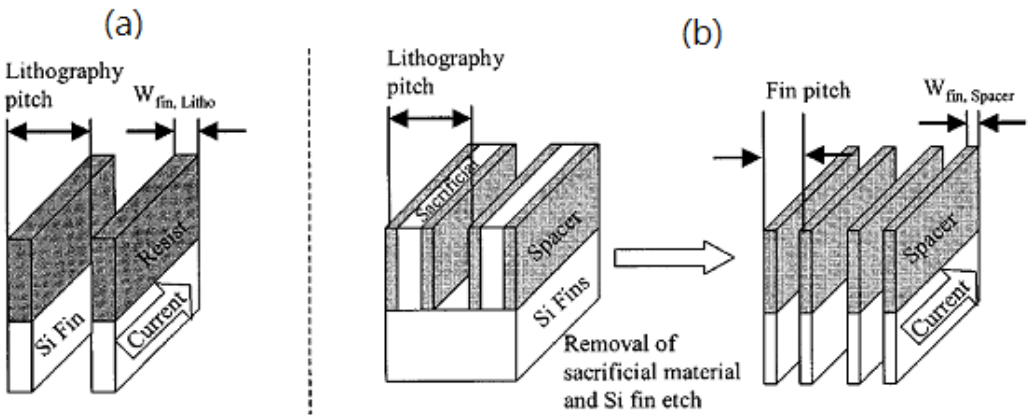

Fig.1-5 The fin density (a) general lithography compare with (b) spacer patterning technology. And the spacer patterning technology can provide double the device density. Adapted from [18]

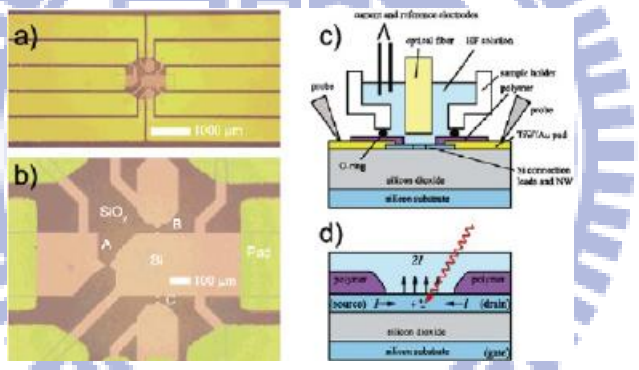

Fig.1-6 Images of sample and setup, with (a) showing the chip layout with gold pads and (b) showing the central device area. The positions of the nanowires are indicated by letters A C. In (c) a schematic cross-section of the etching setup with a mounted sample is shown, and in (d) a schematic cross-section of the nanowire during etching is shown [19].

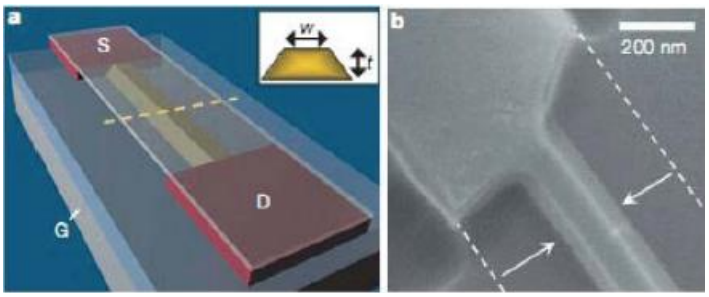

Fig.1-7 (a) schematic after anisotropic etch. The silicon-on-insulator active channel (yellow, width w and thickness t) is undercut etched, whereas degenerate leads (red) are etch-resistant. (b) SEM image of a device [20].

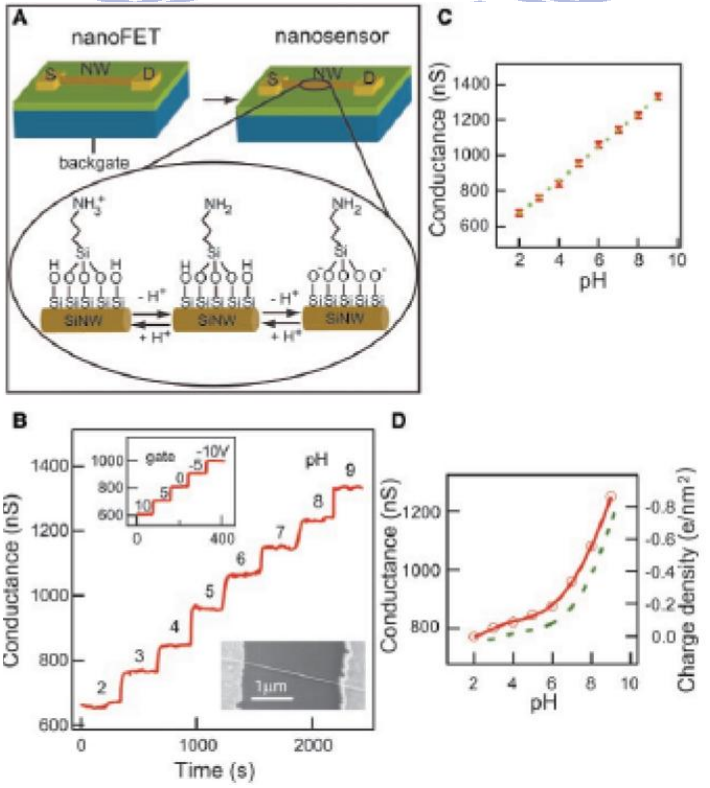

Fig.1-8 (A) Schematic illustrating the conversion of a NWFET into NW pH sensor. (B)Real-time response of an APTES-modified SiNW for pHs from 2 to 9. (C) Plot of the conductance versus pH. (D) The conductance of unmodified SiNW versus pH [20].

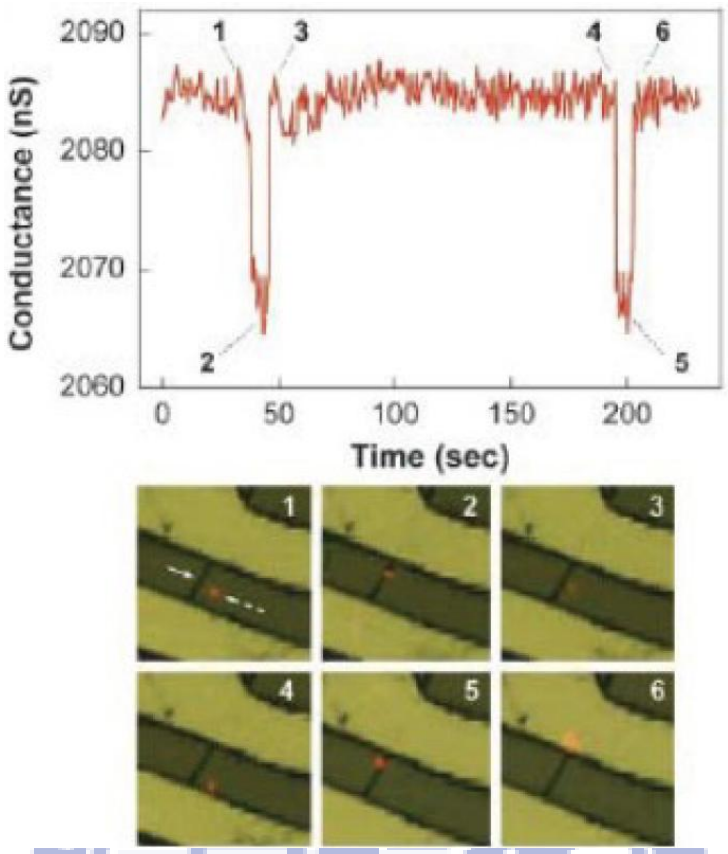

Fig.1-9 Conductance (Upper) and optical (Lower) data recorded simultaneously vs. time for a single silicon nanowire device after introduction of influenza A solution [23].

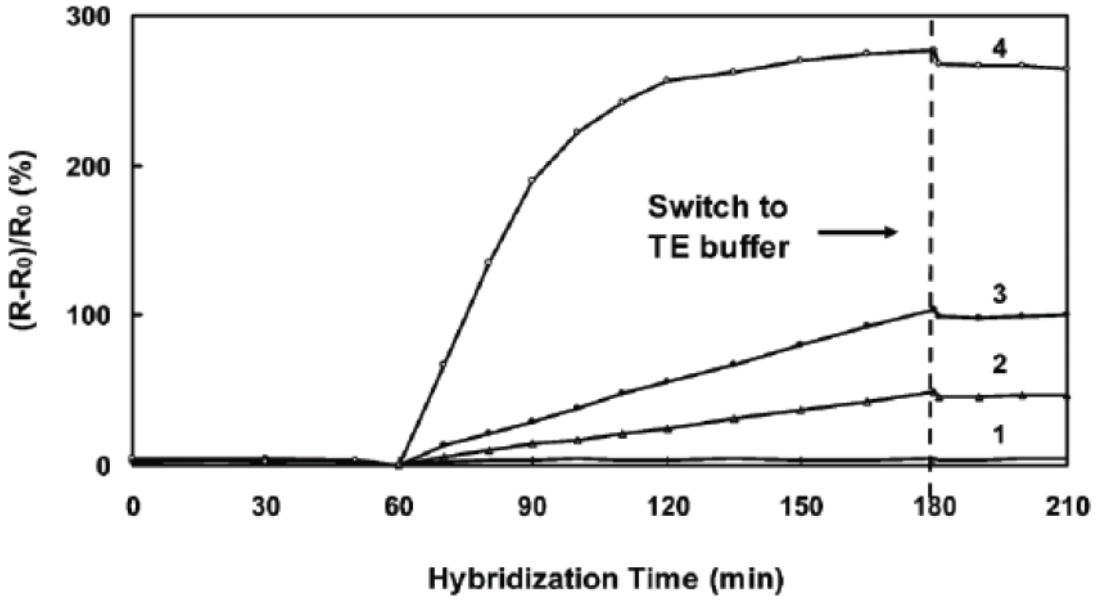

Fig.1-10 The dependence of resistance change of the PNA-functionalized SiNW array on hybridization time in (1) 1.0nM control, (2) 25fM, (3) 100fM, and (4) 1.0nM target DNA in buffer solution.

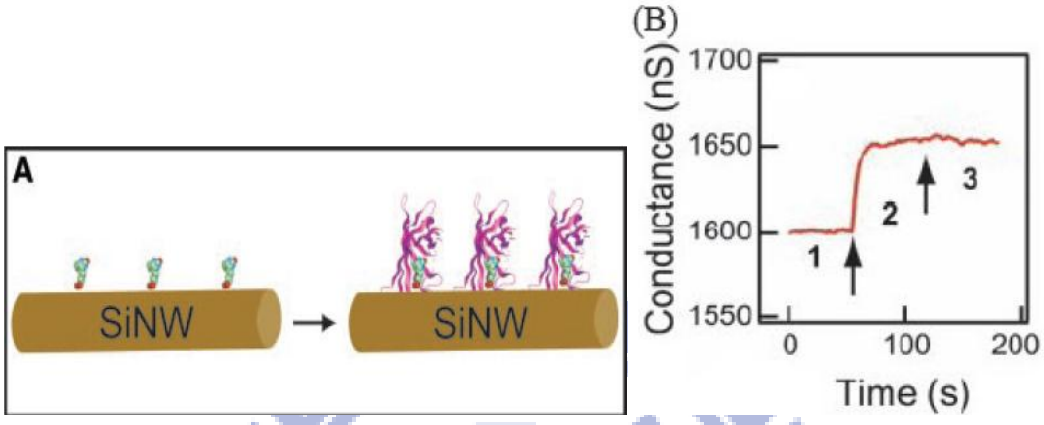

Fig.1-11 (A) A biotin-modified SiNW and subsequent binding of streptavidin to the SiNW surface. (B) Plot of conductance versus time for a biotin-modified SiNW,where region 1 correspond to buffer solution,region 2 corresponds to the addition of 250nM streptavidin[20].

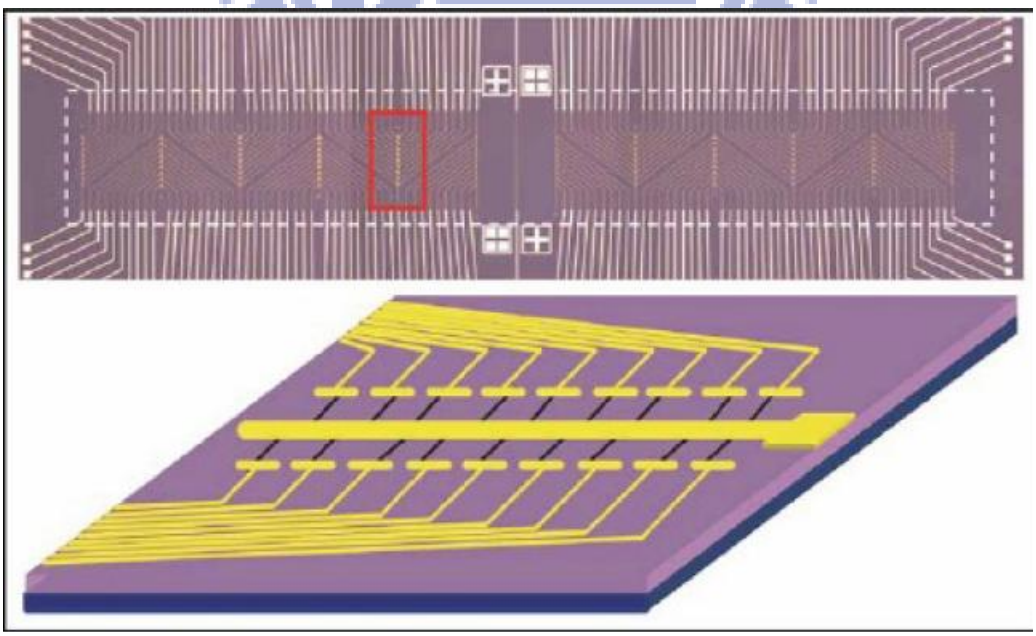

Fig.1-12 Optical image (top) of a nanowire device array. The schematic

illustration (bottom) shows the detail of the red rectangle in the optical image. Golden lines are electrodes connecting nanowires, which is blue lines here [26].

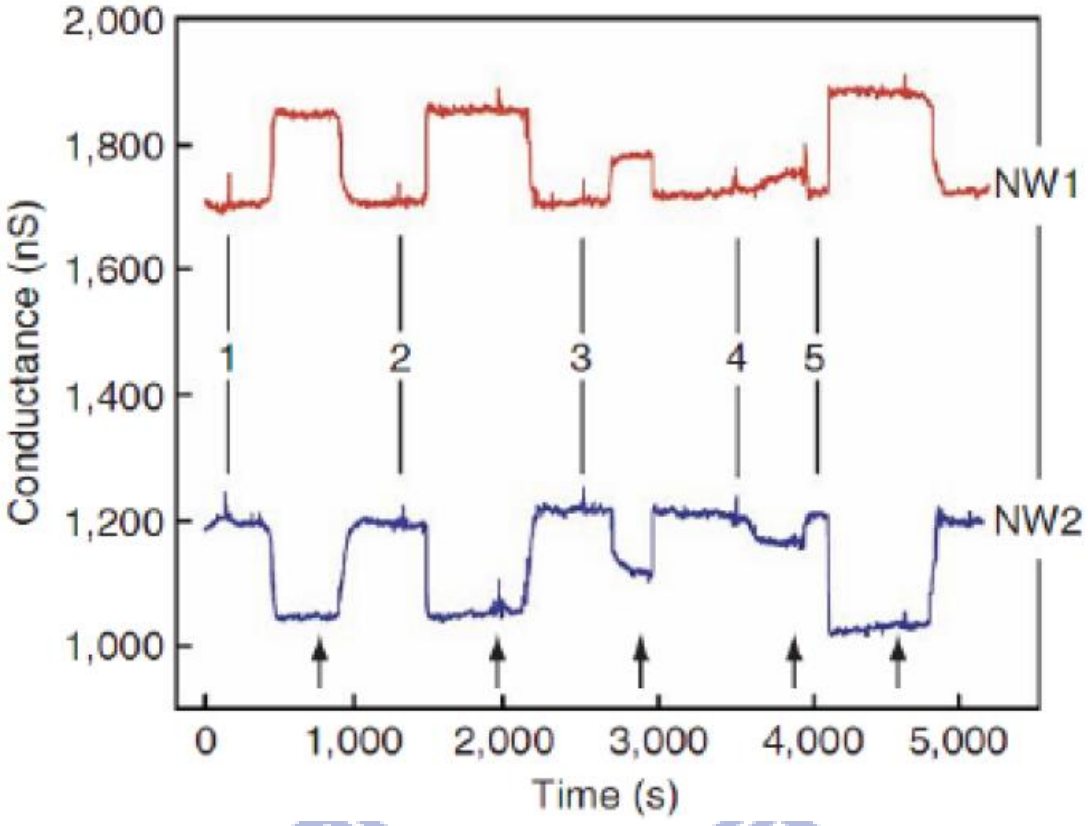

Fig.1-13 Complementary sensing of PSAusing p-type (NW1) and n-type (NW2) silicon-nanowire devices in the same array. [26]

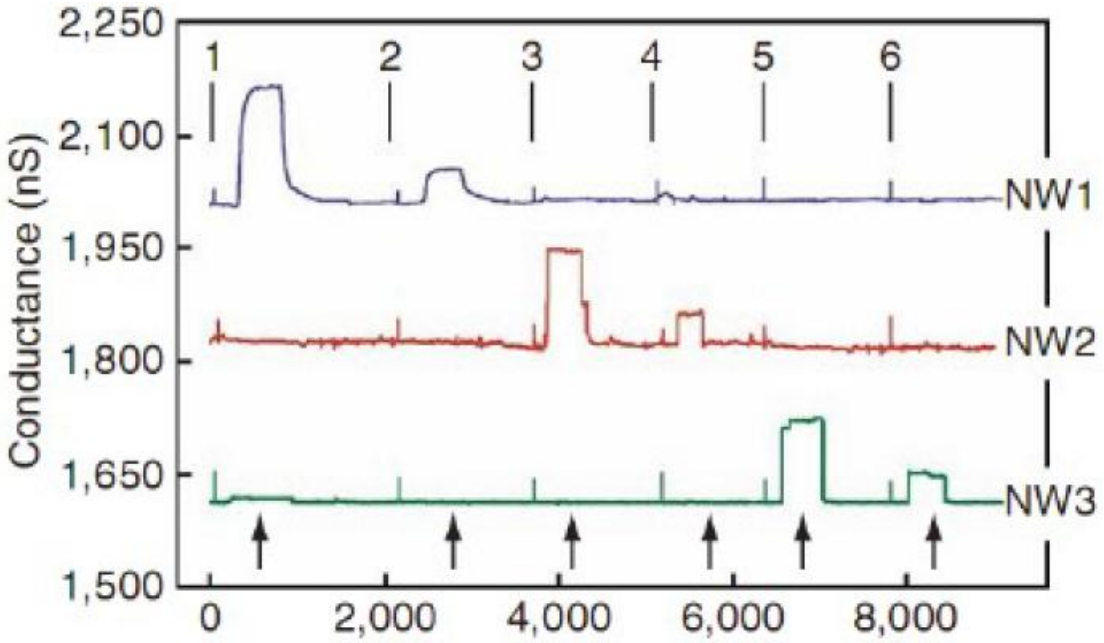

Fig.1-14 Conductance-versus-time data recorded for the simultaneous detection of PSA, CEA and mucin-1 on p-type silicon-nanowire array in which NW1, NW2 and NW3 were functional-ized with mAbs for PSA, CEA and mucin-1, respectively. Thesolutions were delivered to the nanowire array sequentially as follows: 1) 0.9 ng/mL PSA, 2) 1.4 pg/mL PSA, 3) 0.2 ng/mL CEA, 4) 2 pg/mL CEA, 5) 0.5 ng/mL mucin-1, 6) 5 pg/mL mucin-1[26].

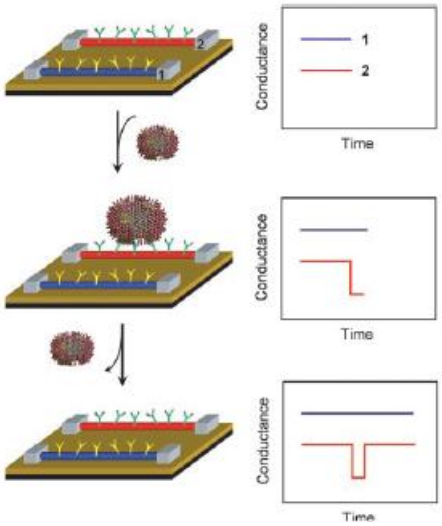

Fig.1-15 NWs detect single viruses. The schematic *Left* shows two NW devices, 1 and 2, where the NWs are modified with different antibody receptors. And the schematic *Right* shows only NW-2 binding with single virus. When the virus unbinds from the surface the conductance returns to the baseline value. [27]

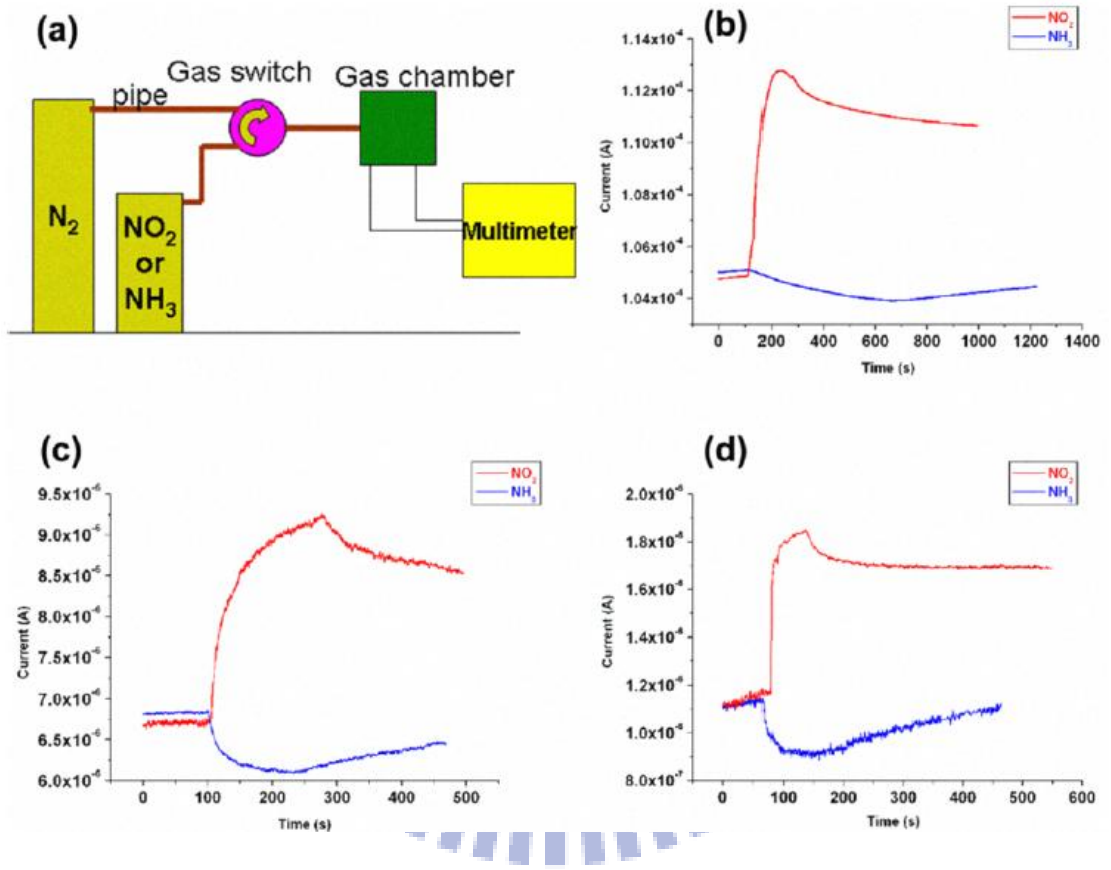

Fig.1-16 (a) The gas sensing system; (b) The thin-film device response with the NO_2 (red curve) and NH_3 (blue curve); (c) The response of 130 nm NW device to NO_2 and NH_3; (d) The response of 75 nm NW device to NO_2 and NH_3. [29]

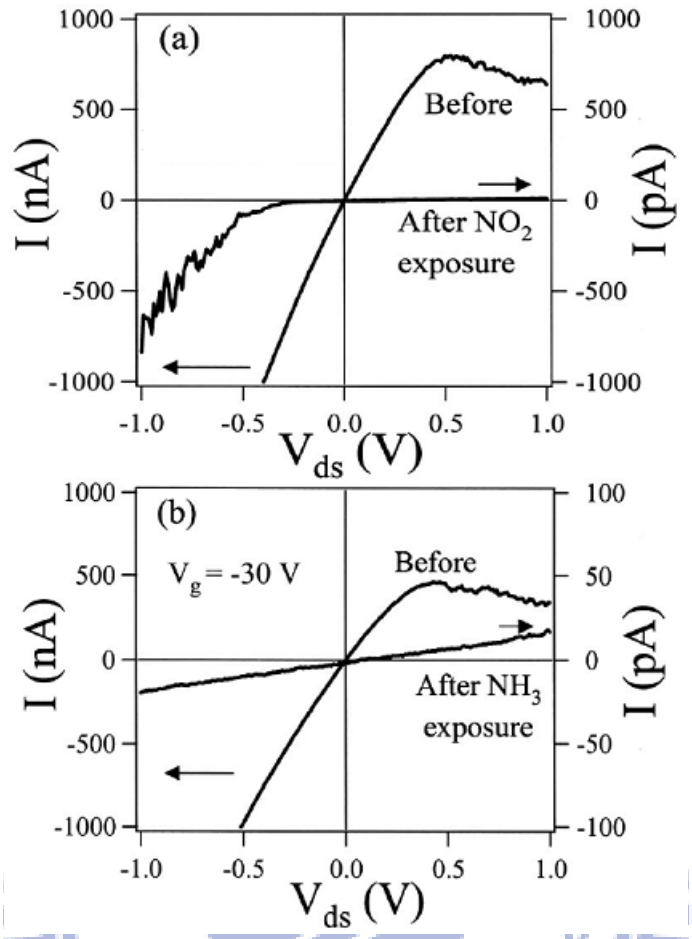

Fig.1-17 (a) *I* –*V* curves measured before and after exposure to 100-ppm NO_2. (b) *I* –*V* curves measured before and after exposure to 1% NH_3 with V_g= -30 V. [37]

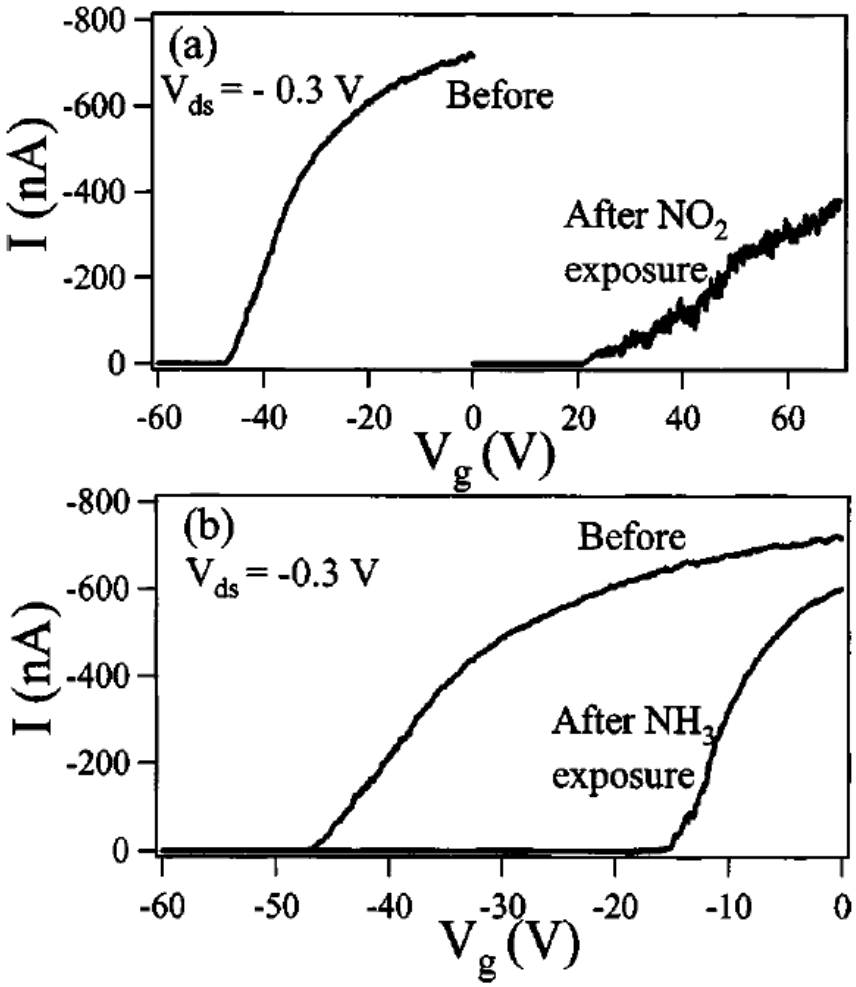

Fig.1-18 The V_{th} shift. Schematic (a) I –V_g curves before and after exposure to 100-ppm NO_2 with V_{ds}=-0.3 V. (b) I –V_g curves before and after exposure to 1% NH_3 with V_{ds}=-0.3 V. [37]

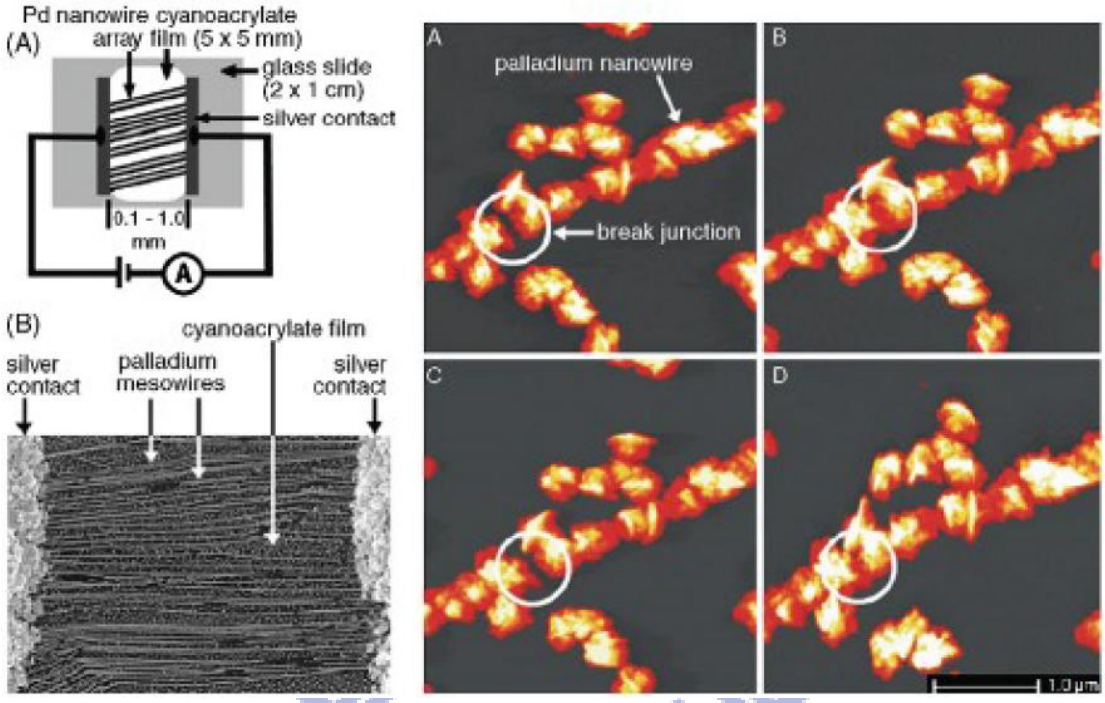

Fig.1-19 (A) Schematic diagram of a PMA-based hydrogen sensor or switch. (B) SEM image of the active area of a PMA-based hydrogen sensor. (Right) Atomic force microscope images of a Pd mesowire on a graphite surface. Images (A) and (C) were acquired in air, and images (B) and (D) were acquired in a stream of hydrogen gas. A hydrogen-actuated break junction is highlighted [40].

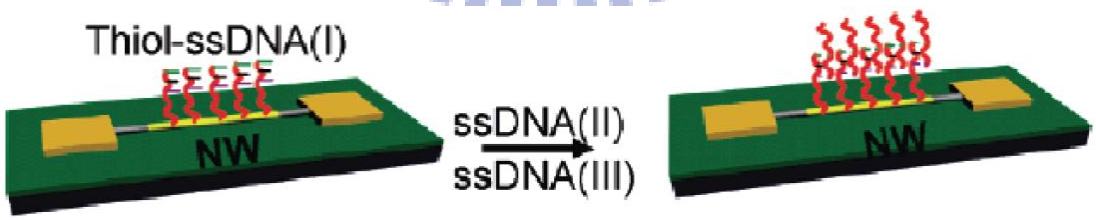

Fig.1-20 Schematic illustration of surface receptors modified CdTe-Au-CdTe nanowire FET for the detection of DNA. Thiolterminated ssDNA(I) binding to the Au segment serves as the surface receptors. [43]

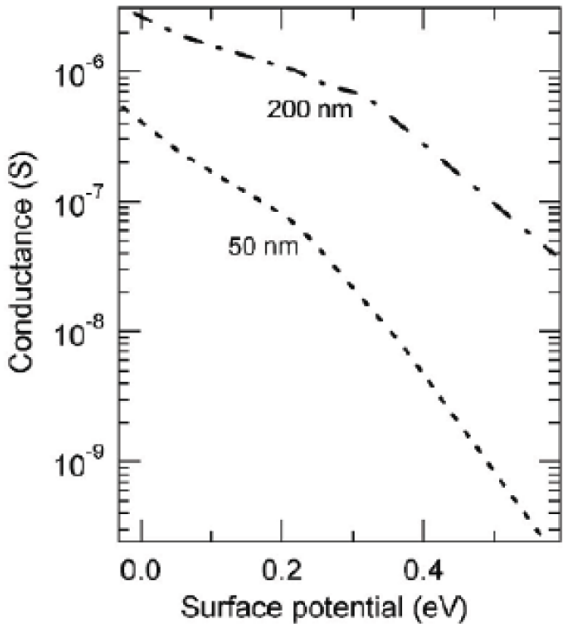

Fig.1-21 Simulated conductance values as a function of the surface potential for the 200-nm-wide and 50-nm-wide wires [44].

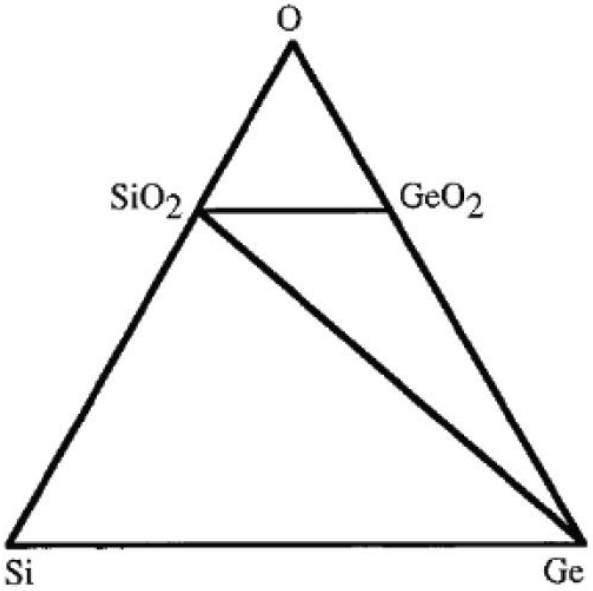

Fig.1-22 Ternary phase diagram for the Si–Ge–O system at 1000 K and 1 bar, calculated based on the thermochemical data. [49]

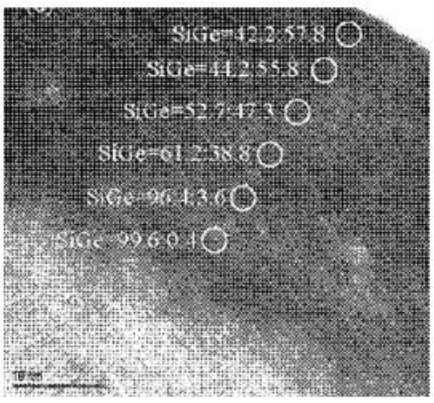

Fig.1-23 TEM image of SiGe layer with 55% Ge without threading dislocations. [50]

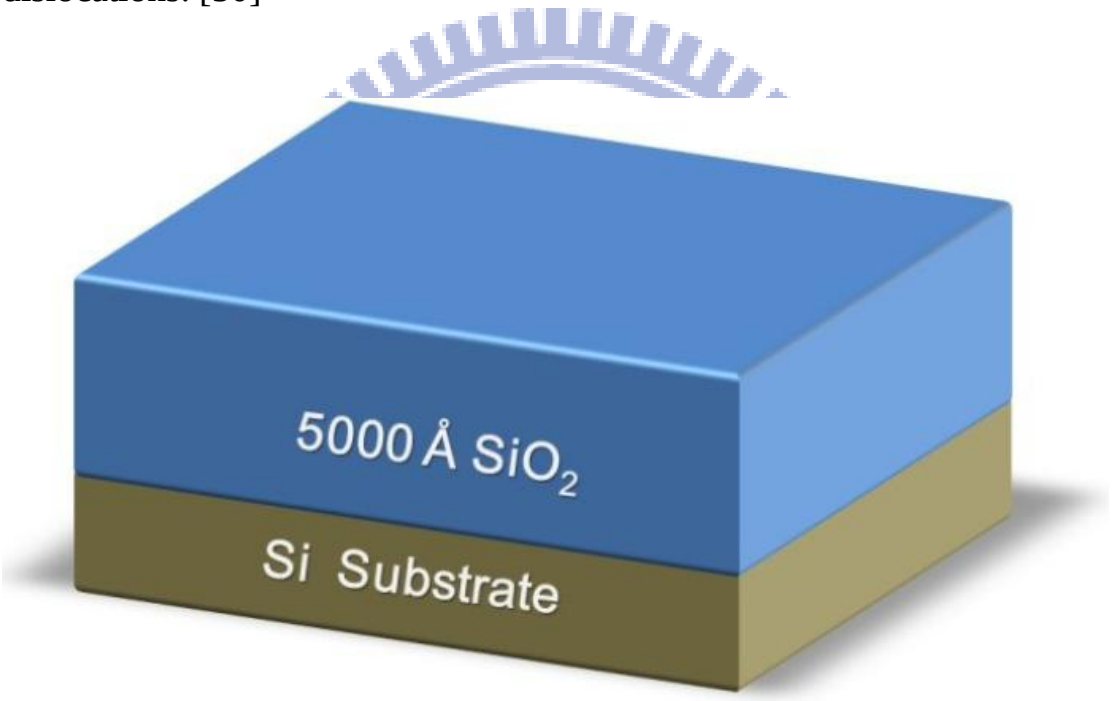

Fig.2-1 5000 Å SiO2 layer was grown on Si substrate.

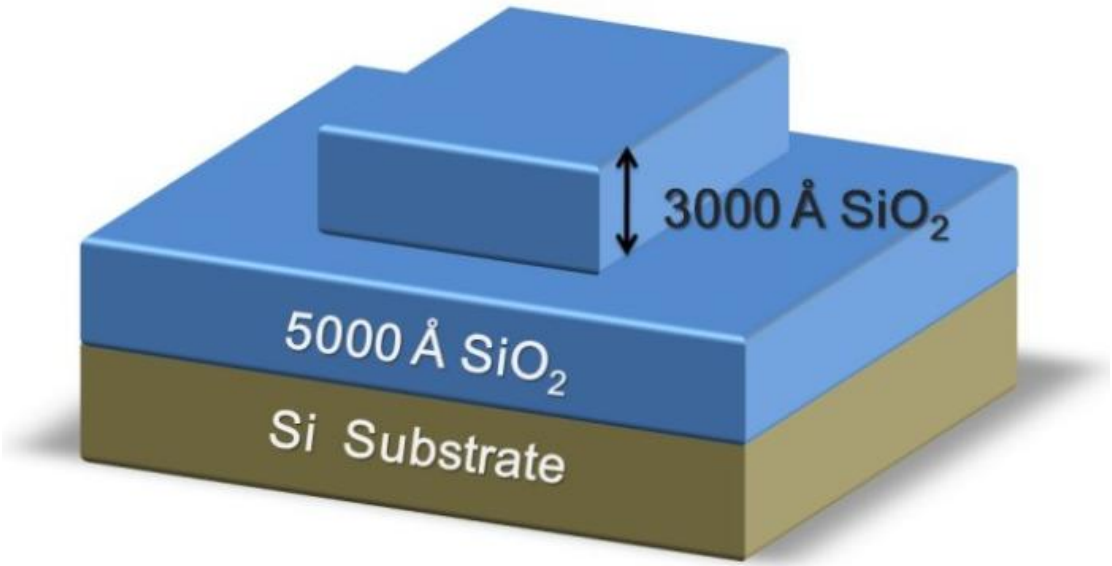

Fig.2-2 Defined of the active area. The height of oxide step is 3000Å .

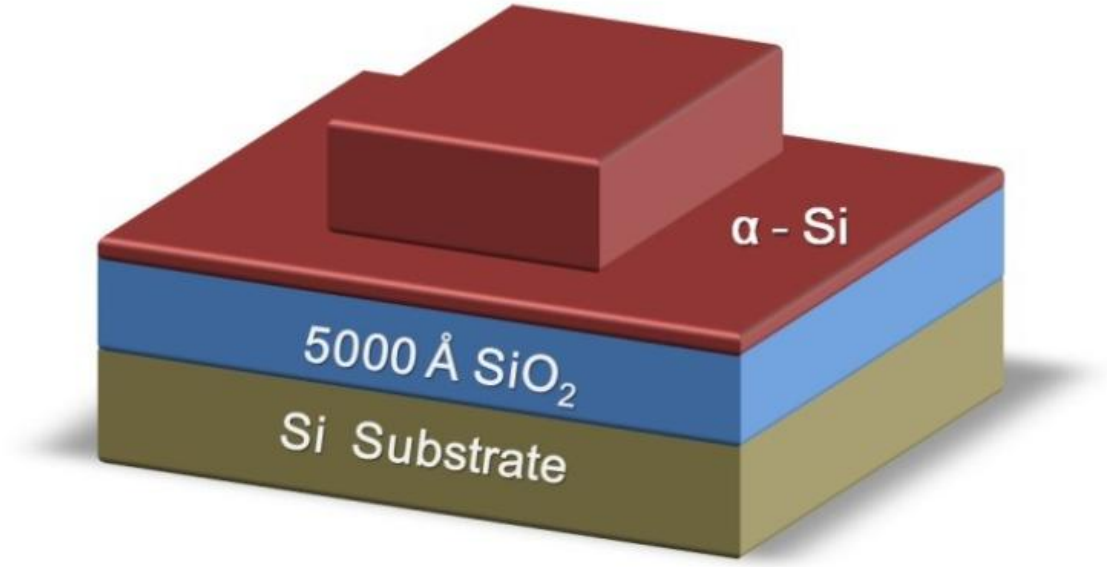

Fig.2-3 200 Å amorphous Si layer is deposited on SiO2 layer.

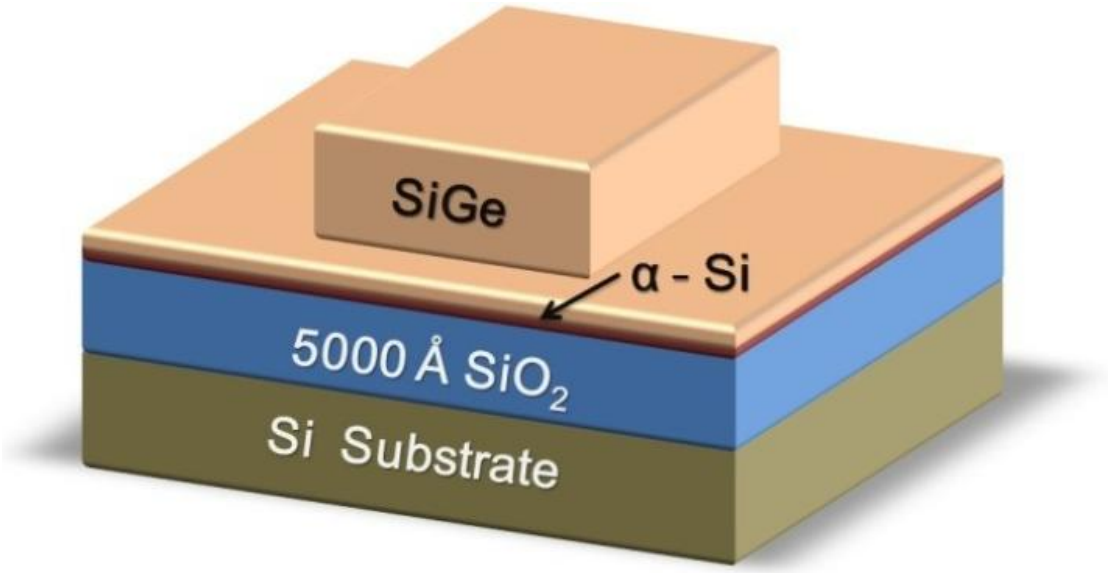

Fig.2-4 SiGe films with different Ge concentration were deposited on α-Si layer.

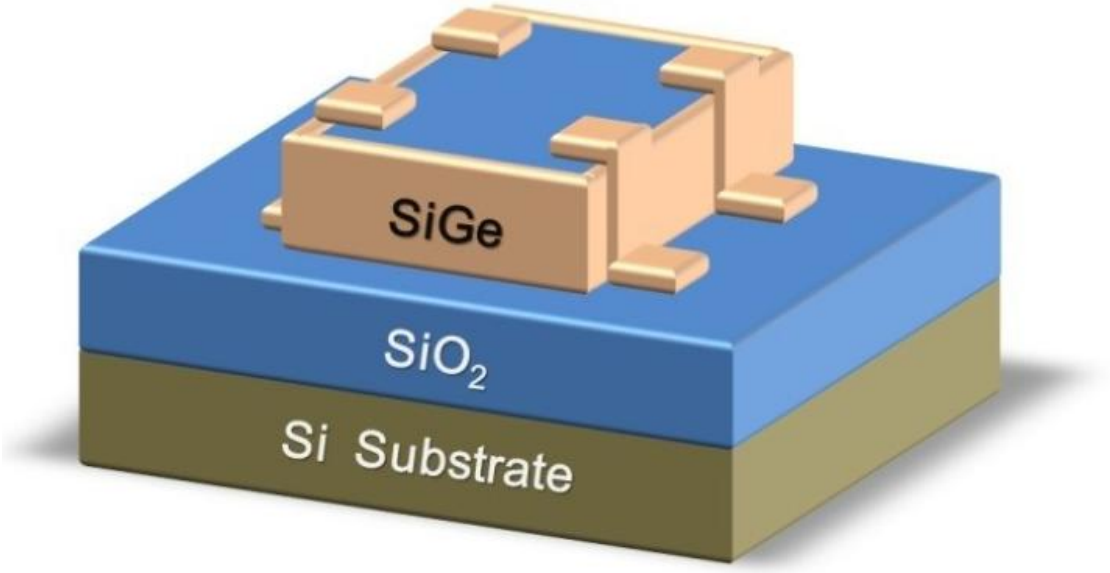

Fig.2-5 The definition of the S/D region and nanowire.

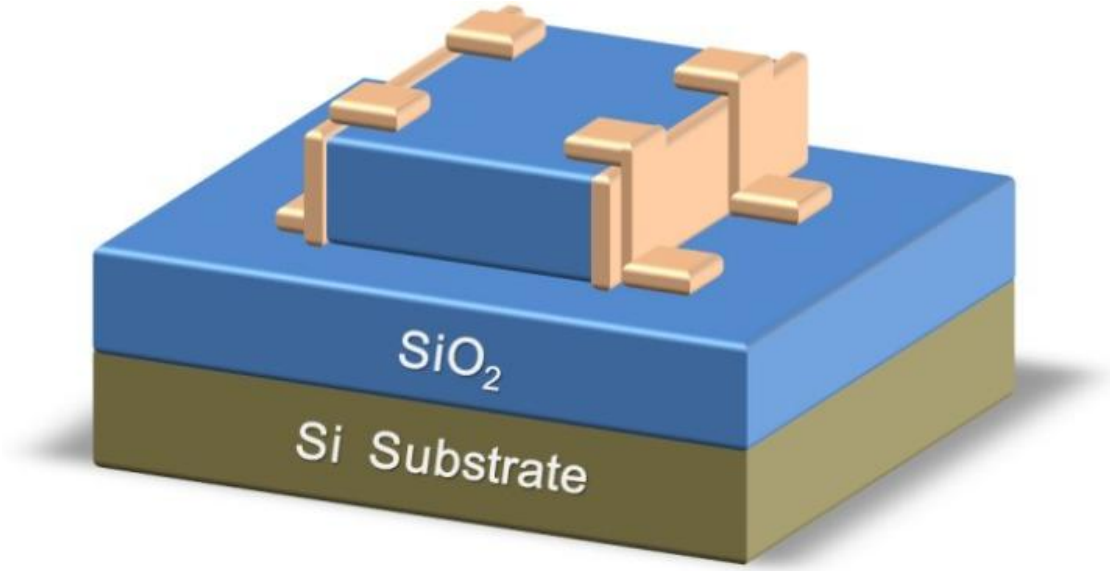

Fig.2-6 Remove one side of the parallel SiGe spacer to cut off the leakage current.

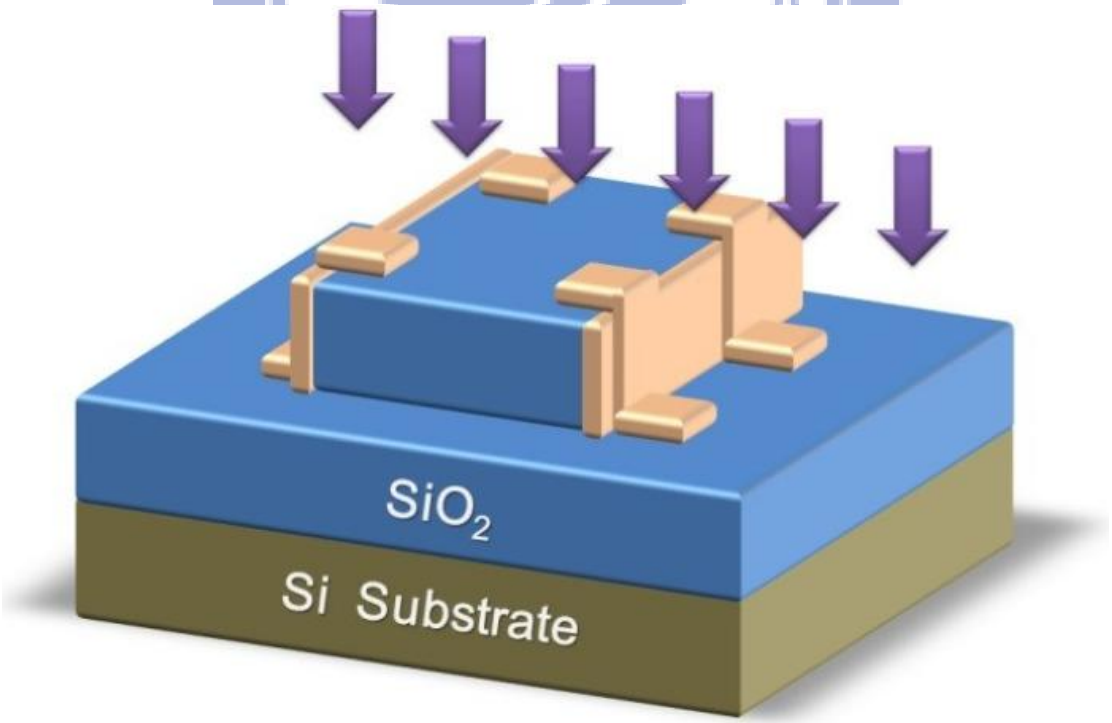

Fig.2-7 Boron - fluoride (BF2) ion implantation.

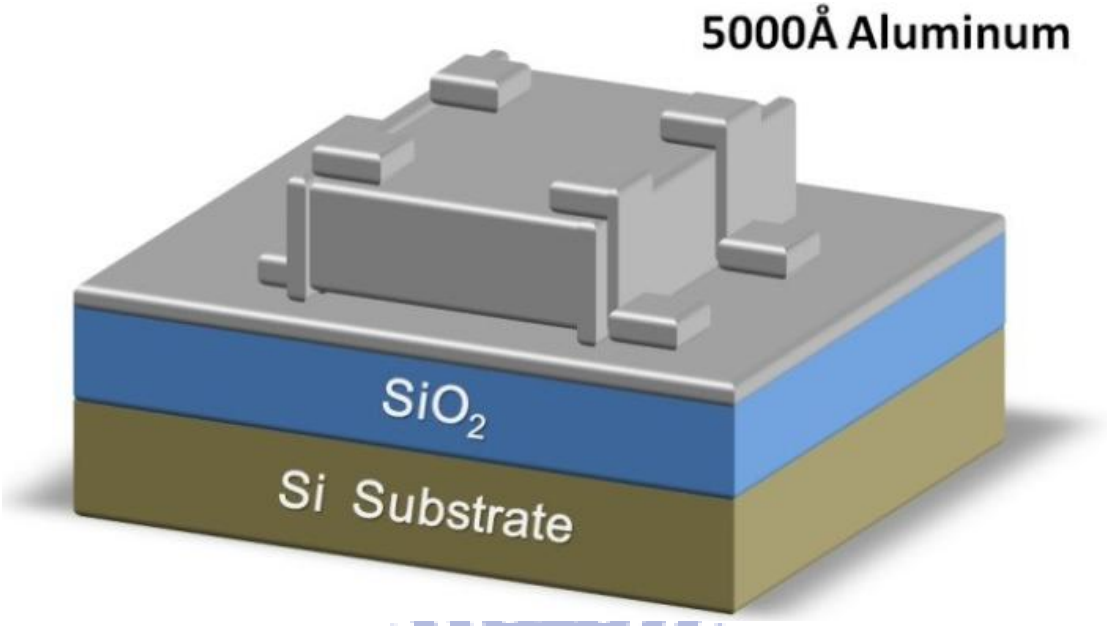

Fig.2-8 5000Å Aluminum deposition.

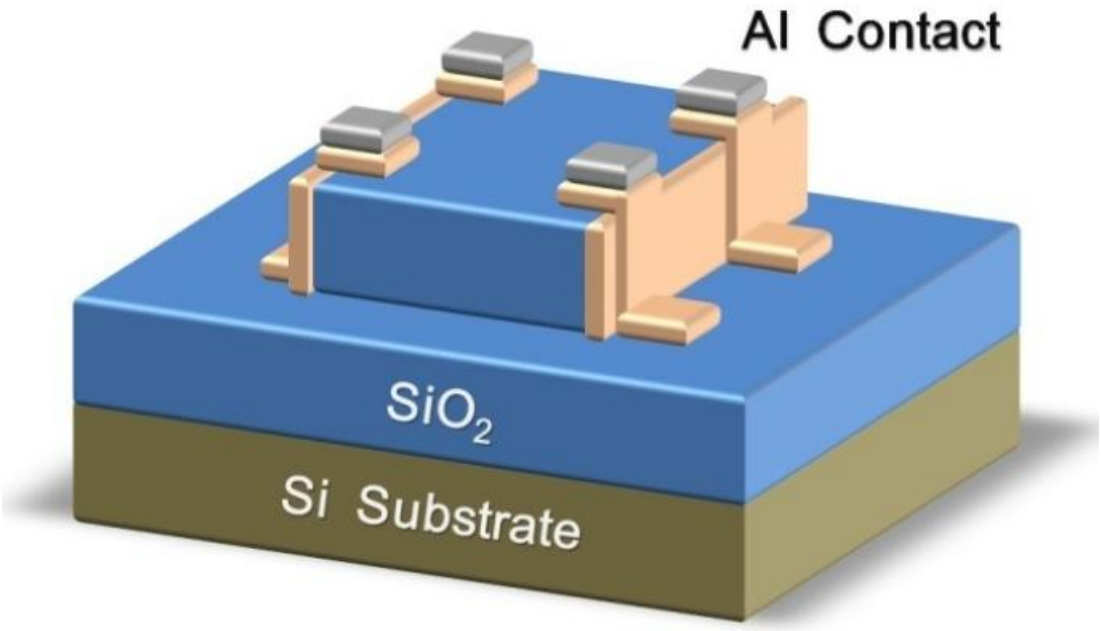

Fig.2-9 Defined Al contact pad.

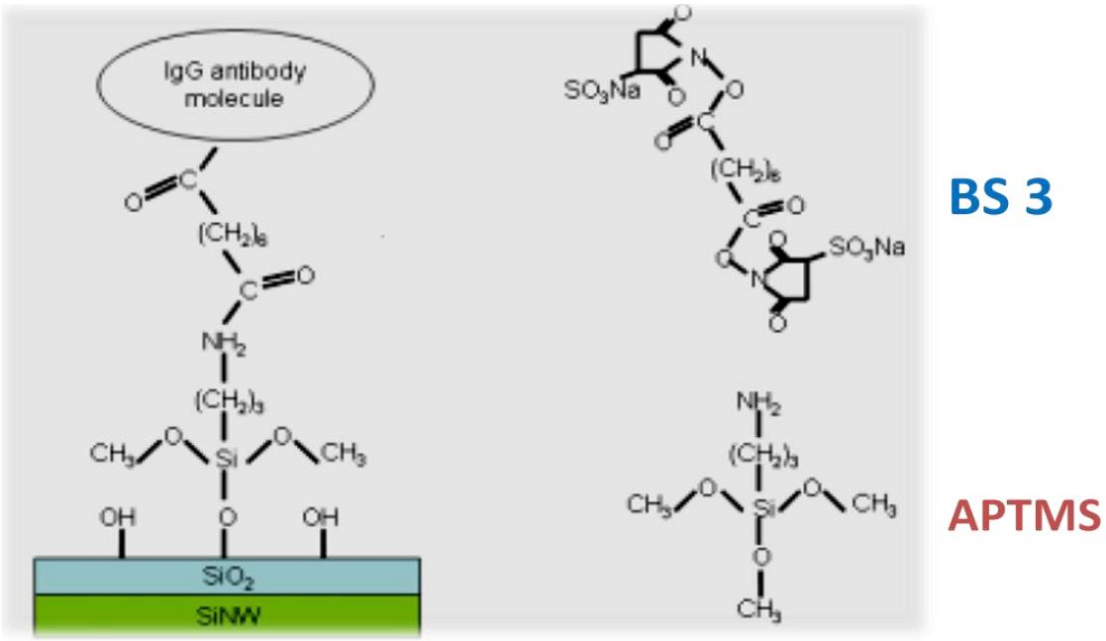

Fig.2-10 The modification of surface by APTMS and linked by BS3.

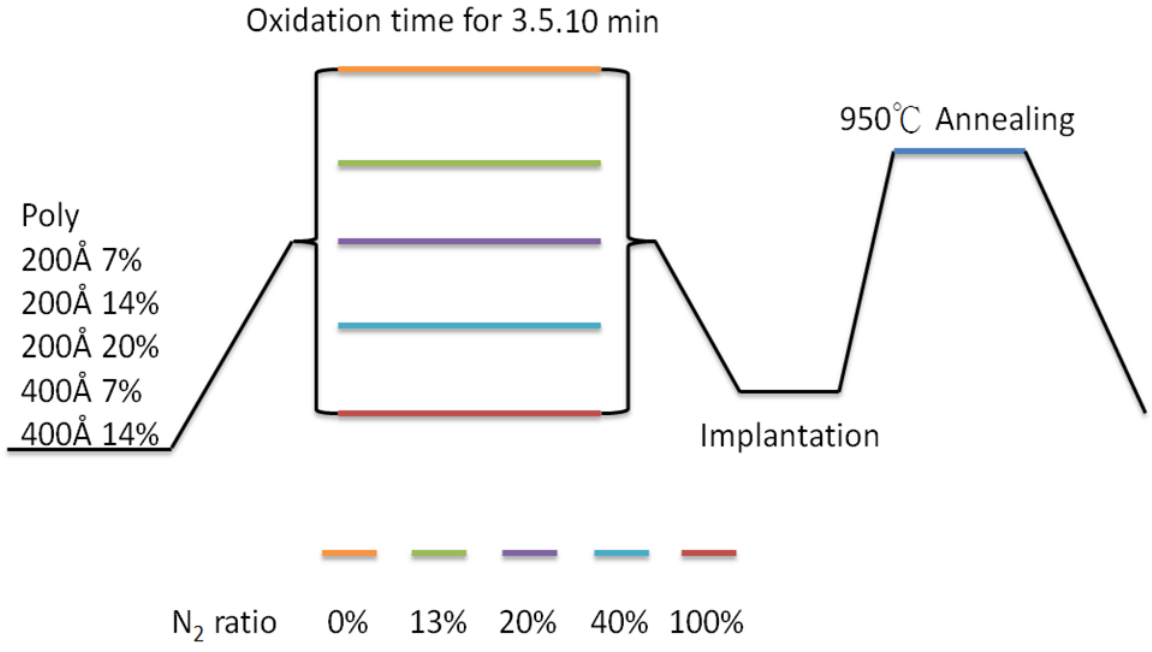

Fig.3-1 The oxidation of stacked structures under different combination of Nitrogen and Oxygen. But for the ratio of N_2 is 100% has no the procedure of oxidation for 5.10min.

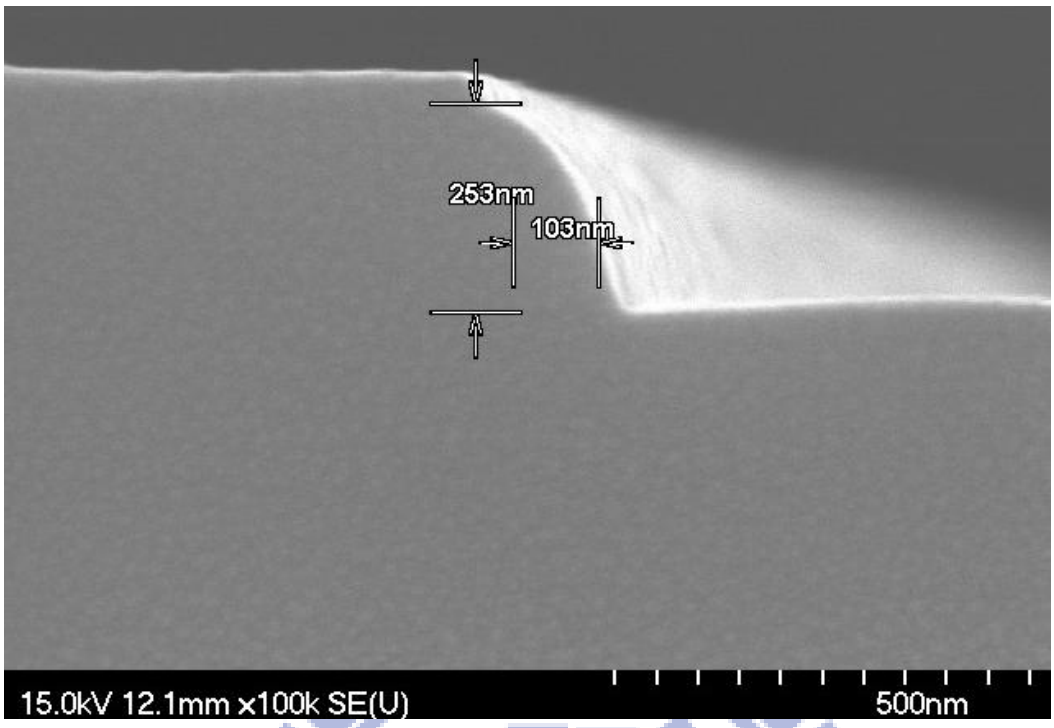

Fig.3-2 SEM images of Poly-Si nanowire.

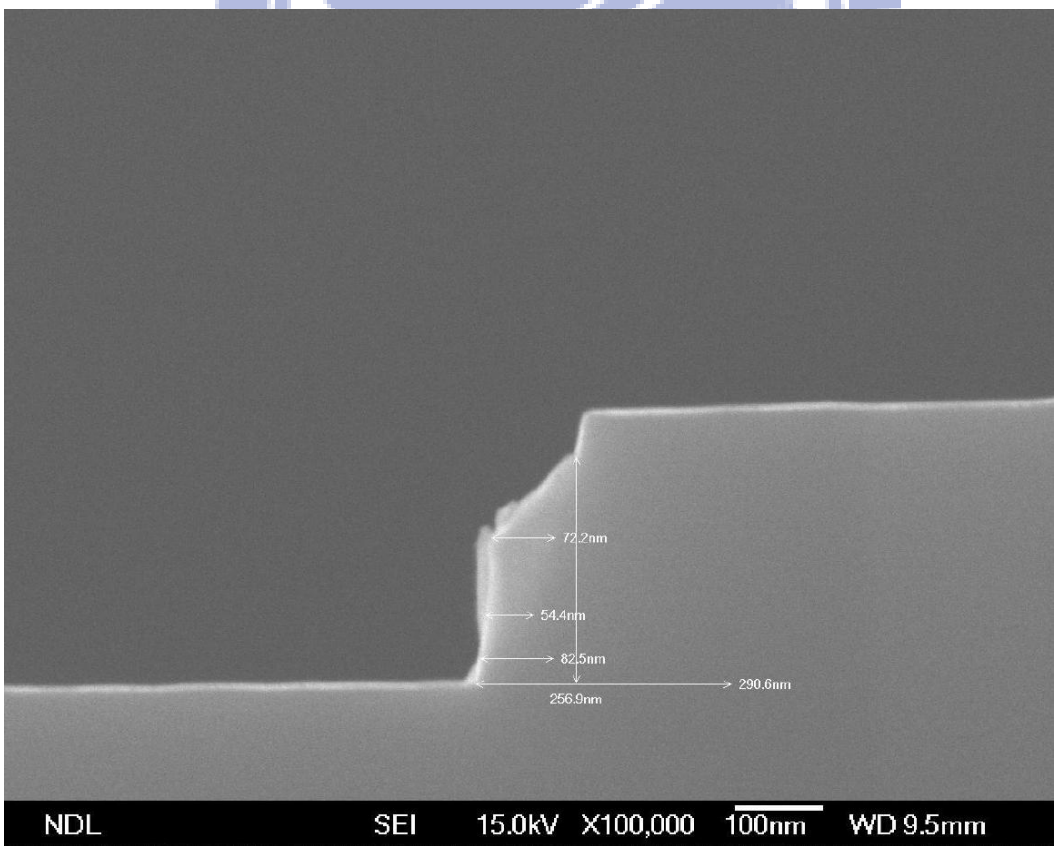

Fig.3-3 SEM images of amorphous Si 200Å and 7% of Ge concentration.

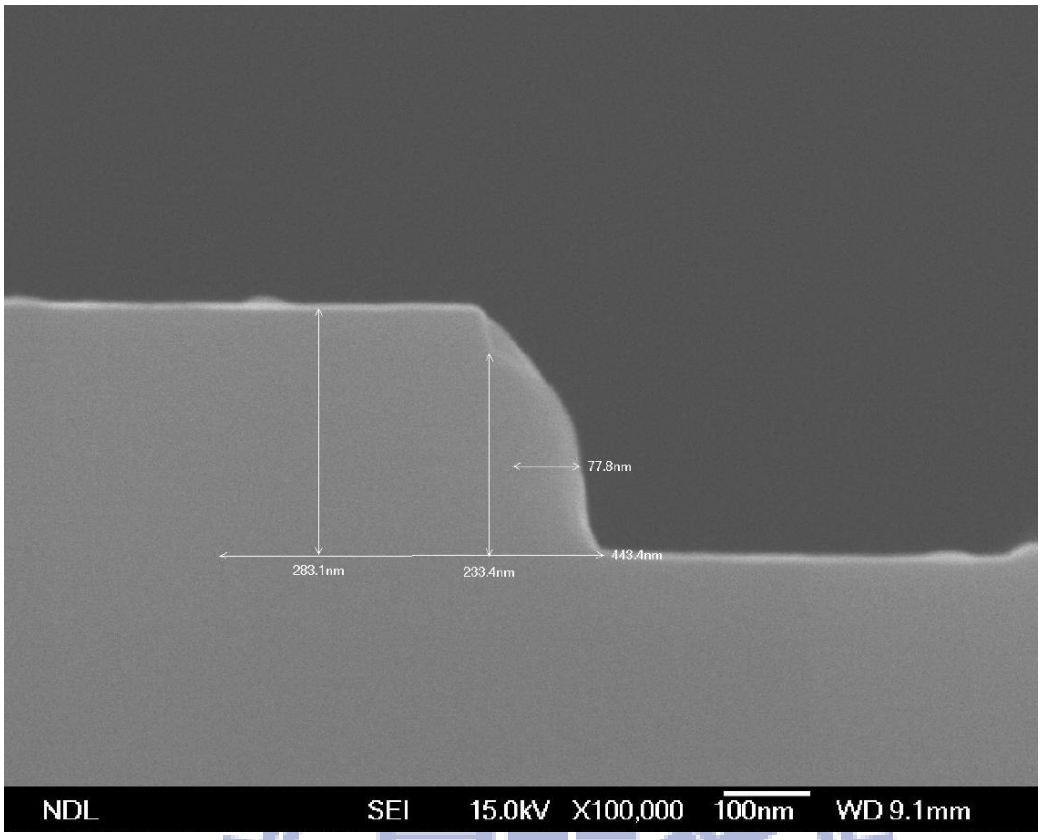

Fig.3-4 SEM images of amorphous Si 200Å and 14% of Ge concentration.

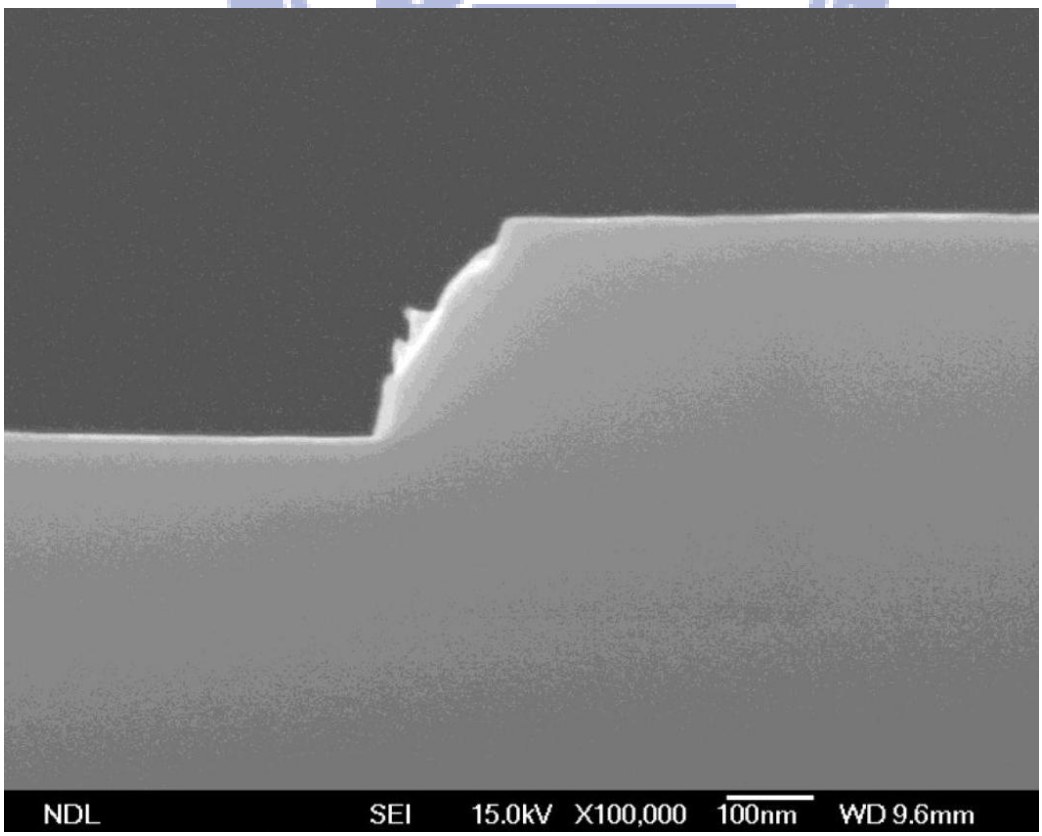

Fig.3-5 SEM images of amorphous Si 200Å and 20% of Ge concentration.

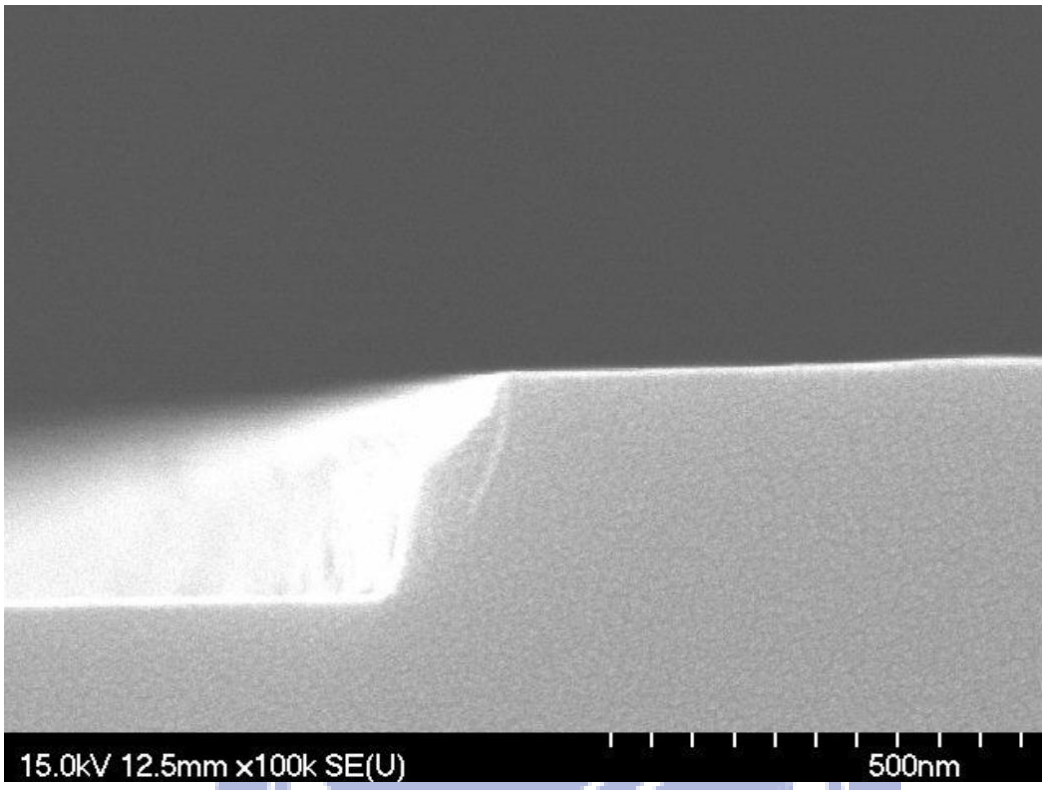

Fig.3-6 SEM images of amorphous Si 400Å and 7% of Ge concentration.

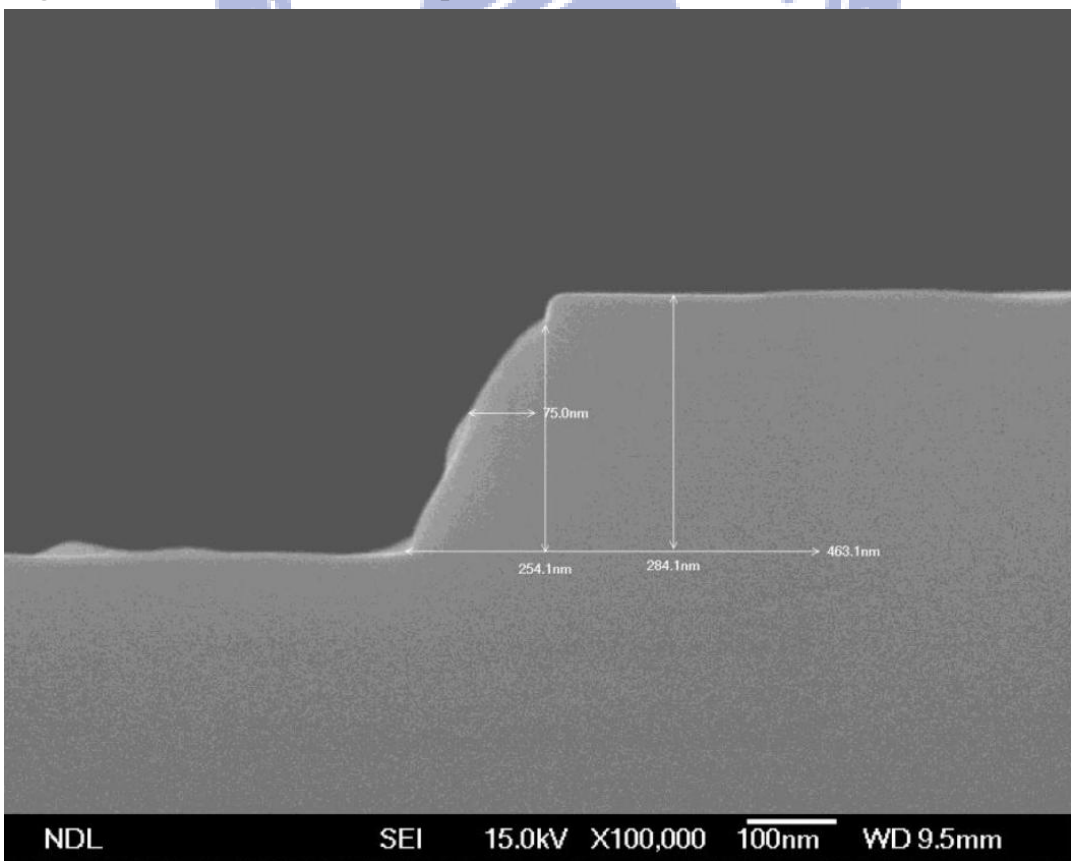

Fig.3-7 SEM images of amorphous Si 400Å and 14% of Ge concentration.

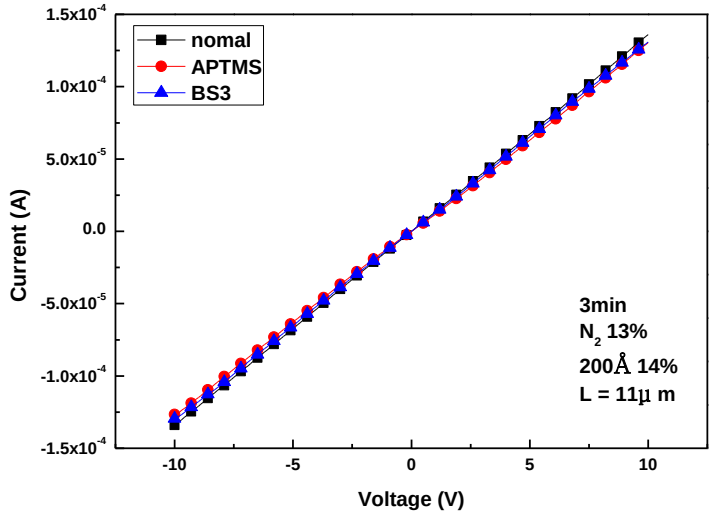

Fig.3-8 I-V characteristic curves of $Si_{0.86}Ge_{0.14}$ NWs with 13% Nitrogen at 900℃ after 3 minutes of oxidation.

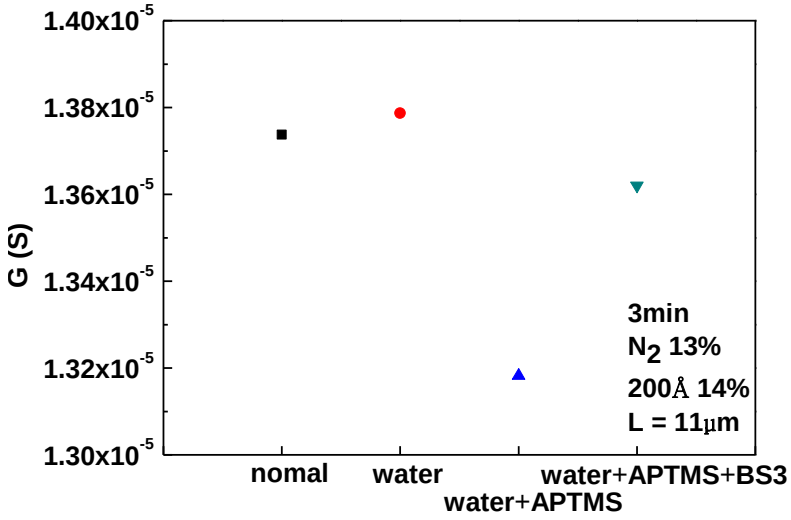

Fig.3-9 The variation of conductivity when the SiGeNW was drop by water, APTMS, and BS3.

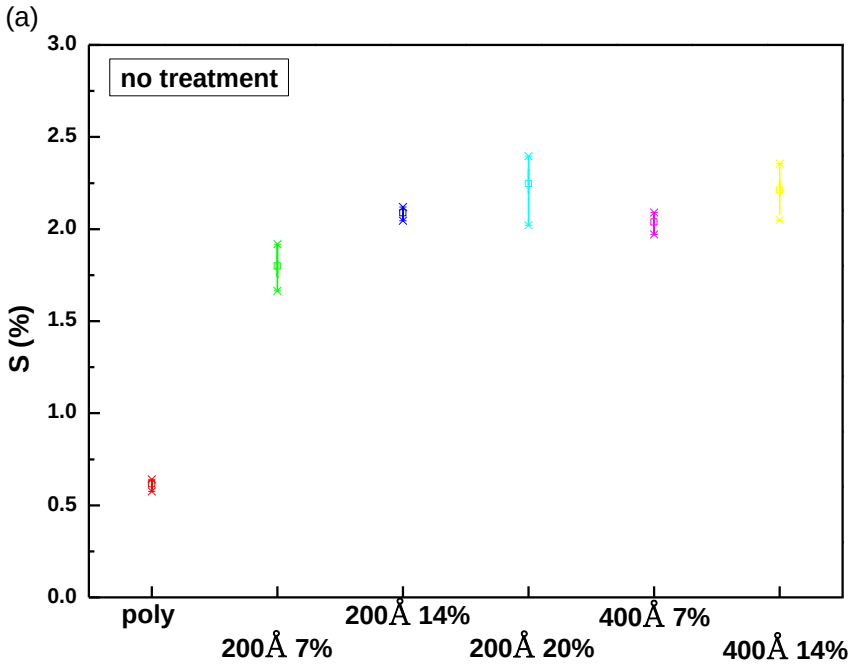

Fig.3-10 The schematic (a) was sensitivity of different stack structures do no any treatment.

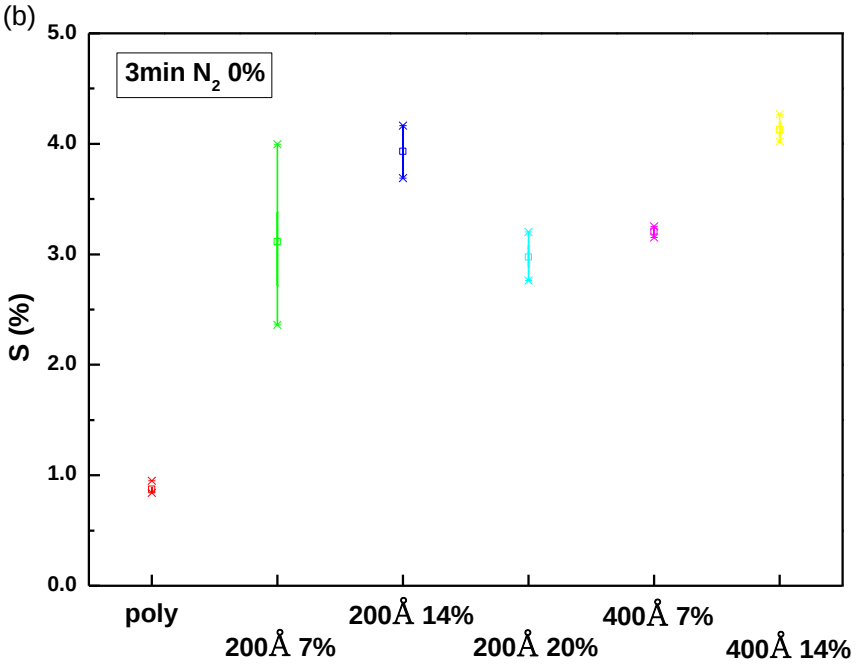

Fig.3-10 The sensitivity of different stack structures for 3min oxidation in different nitrogen/oxygen ratio, and the schematic (b) the ratio of N_2 was 0%.

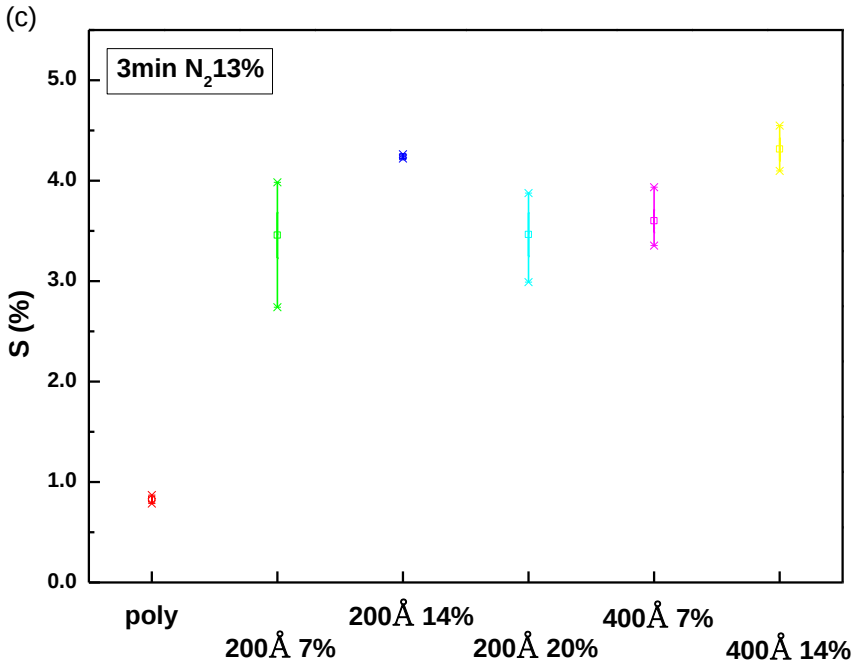

Fig.3-10 The sensitivity of different stack structures for 3min oxidation in different nitrogen/oxygen ratio, and the schematic (c) the ratio of N_2 was 13%.

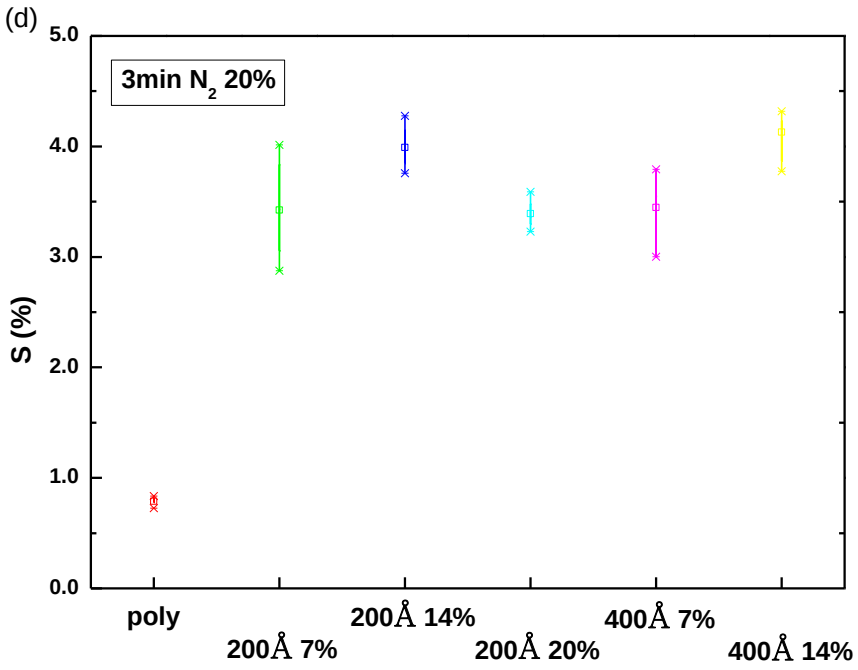

Fig.3-10 The sensitivity of different stack structures for 3min oxidation in different nitrogen/oxygen ratio, and the schematic (d) the ratio of N_2 was 20%.

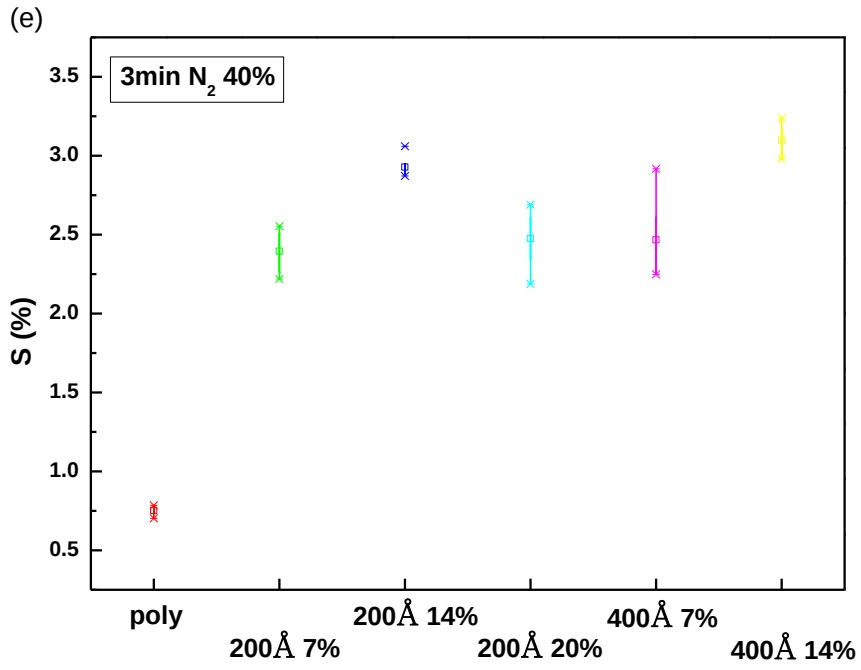

Fig.3-10 The sensitivity of different stack structures for 3min oxidation in different nitrogen/oxygen ratio, and the schematic (e) the ratio of N_2 was 40%.

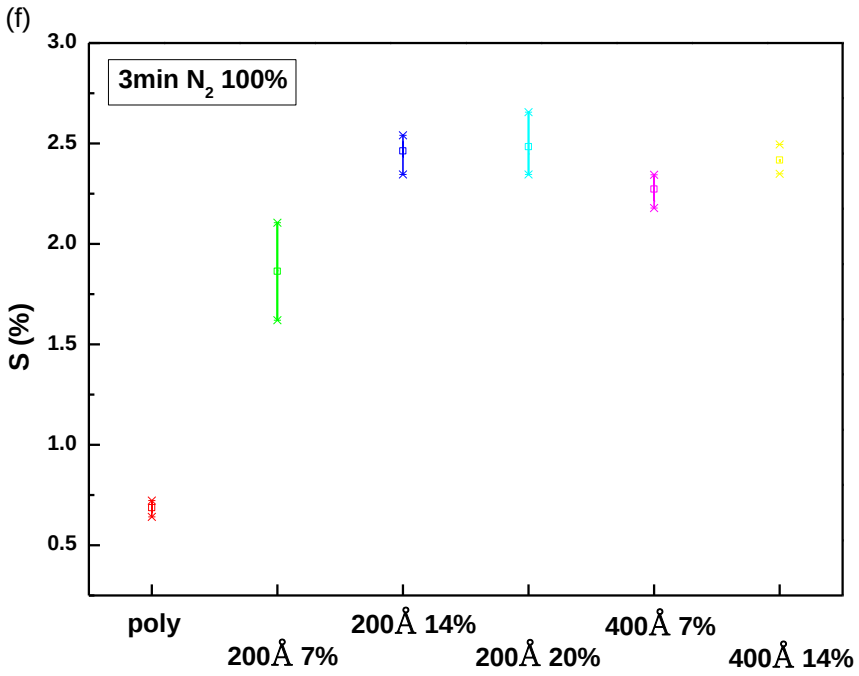

Fig.3-10 The sensitivity of different stack structures for 3min oxidation in different nitrogen/oxygen ratio, and the schematic (f) the ratio of N_2 was 100%.

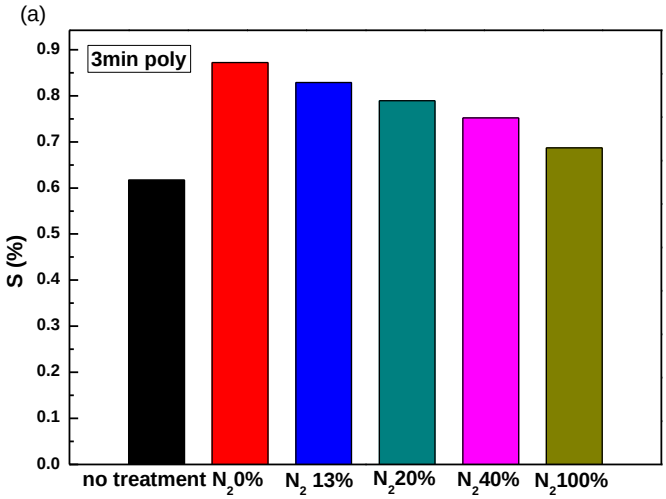

Fig.3-11 The sensitivity in varied nitrogen/oxygen ratio in different stack structure, schematic (a) is Poly-SiNW.

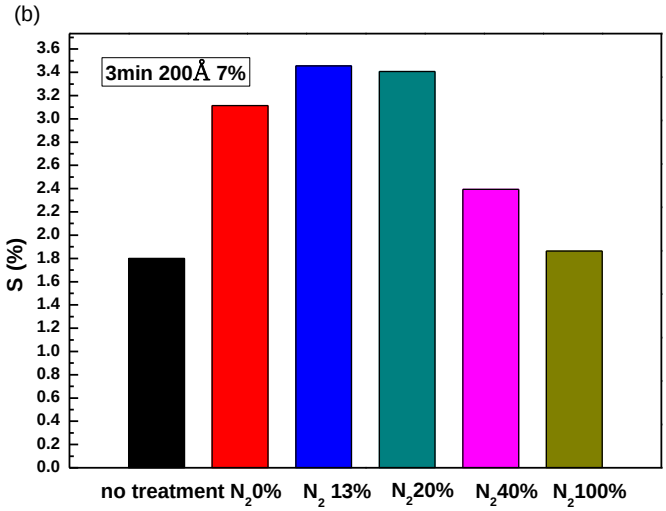

Fig.3-11 The sensitivity in varied nitrogen/oxygen ratio in different stack structure, schematic (b) is α-Si 200Å $Si_{0.93}Ge_{0.07}$.

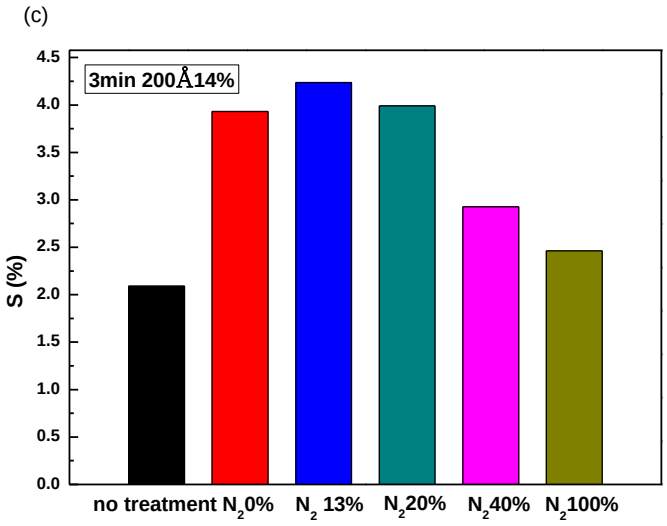

Fig.3-11 The sensitivity in varied nitrogen/oxygen ratio in different stack structure, schematic (c) is α-Si 200Å $Si_{0.86}Ge_{0.14}$.

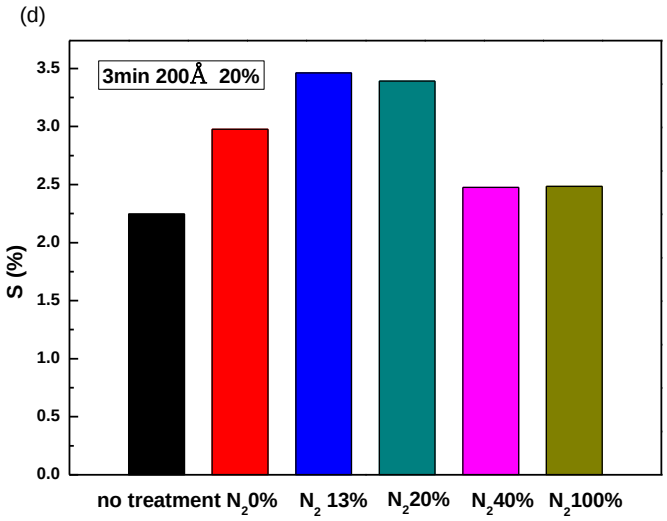

Fig.3-11 The sensitivity in varied nitrogen/oxygen ratio in different stack structure, schematic (d) is α-Si 200Å $Si_{0.80}Ge_{0.20}$.

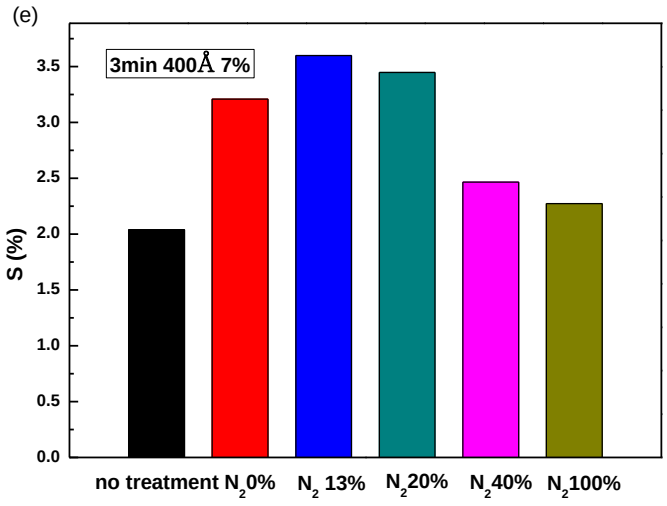

Fig.3-11 The sensitivity in varied nitrogen/oxygen ratio in different stack structure, schematic (e) is α-Si 400Å $Si_{0.93}Ge_{0.07}$.

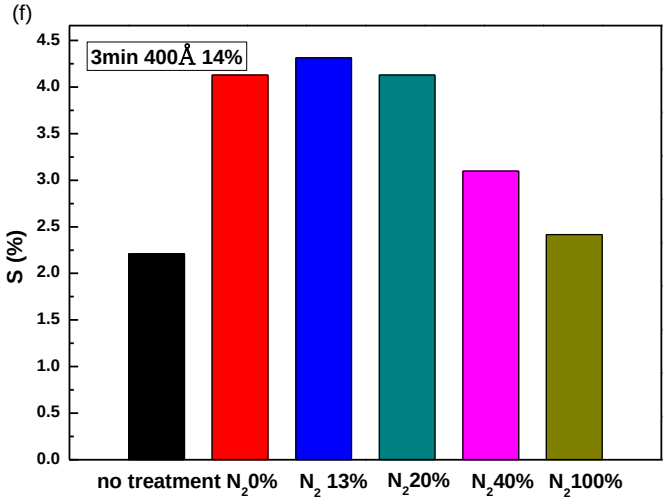

Fig.3-11 The sensitivity in varied nitrogen/oxygen ratio in different stack structure, schematic (e) is α-Si 400Å $Si_{0.86}Ge_{0.14}$.

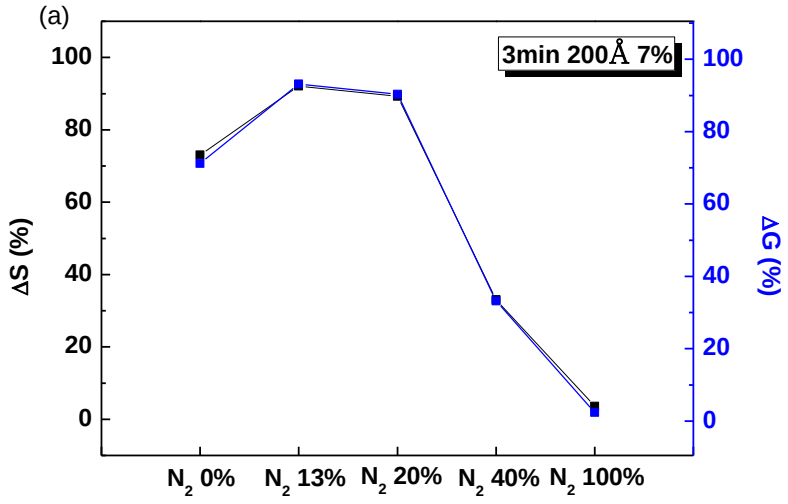

Fig.3-12 The percentage of change amount of sensitivity and conductivity for 3min oxidation for (a) 200Å 7%.

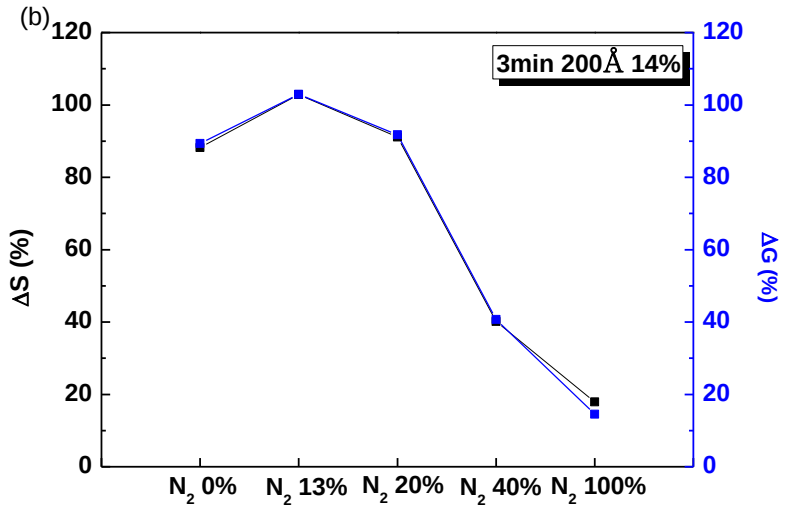

Fig.3-12 The percentage of change amount of sensitivity and conductivity for 3min oxidation for (b) 200Å 14%.

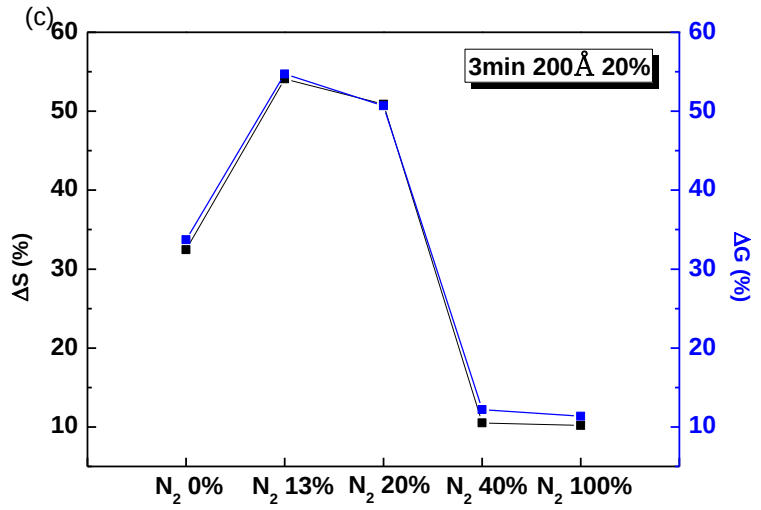

Fig.3-12 The percentage of change amount of sensitivity and conductivity for 3min oxidation for (c) 200Å 20%.

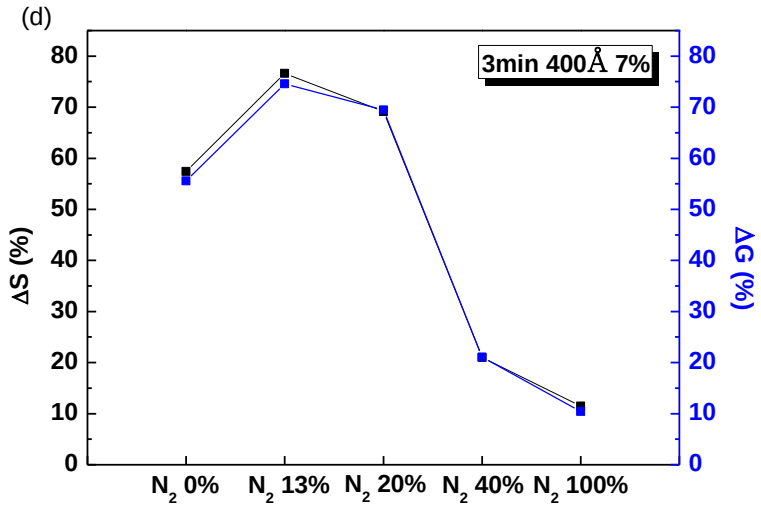

Fig.3-12 The percentage of change amount of sensitivity and conductivity for 3min oxidation for (d) 400Å 7%.

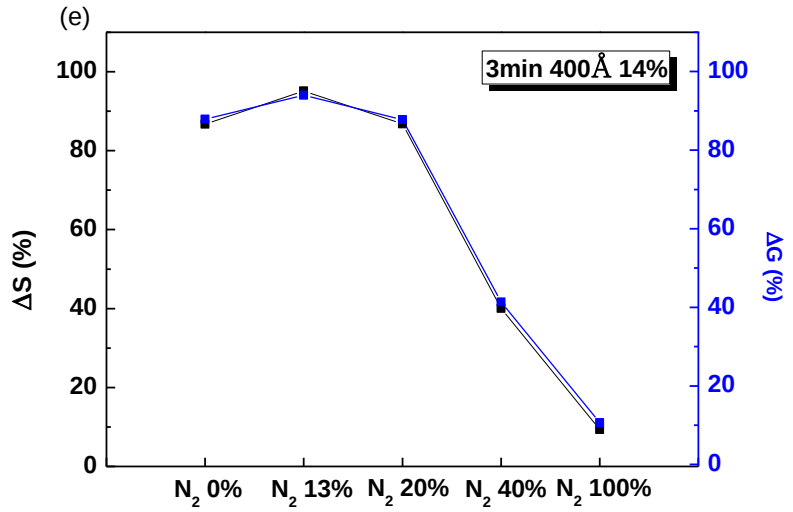

Fig.3-12 The percentage of change amount of sensitivity and conductivity for 3min oxidation for (e) 400Å 14%.

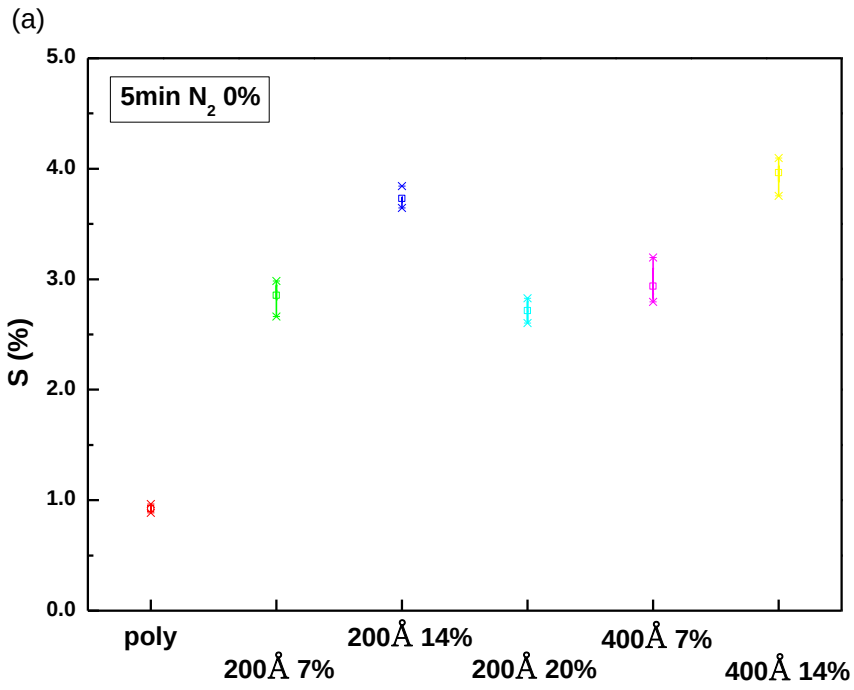

Fig.3-13 The sensitivity of different stack structure for 5min oxidation in different nitrogen/oxygen ratio, (a) the ratio of N_2 was 0%.

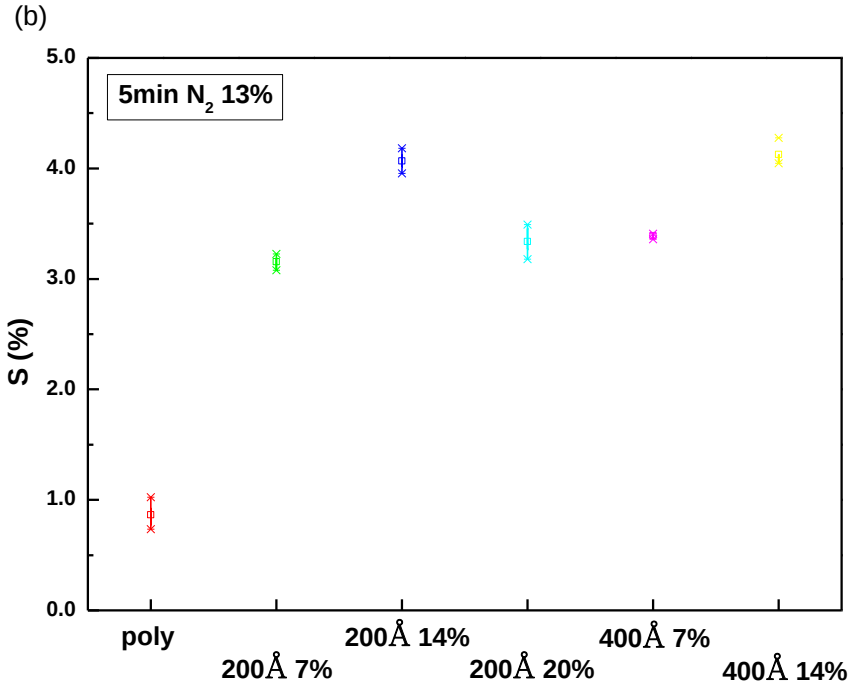

Fig.3-13 The sensitivity of different stack structure for 5min oxidation in different nitrogen/oxygen ratio, (b) the ratio of N_2 was 13%.

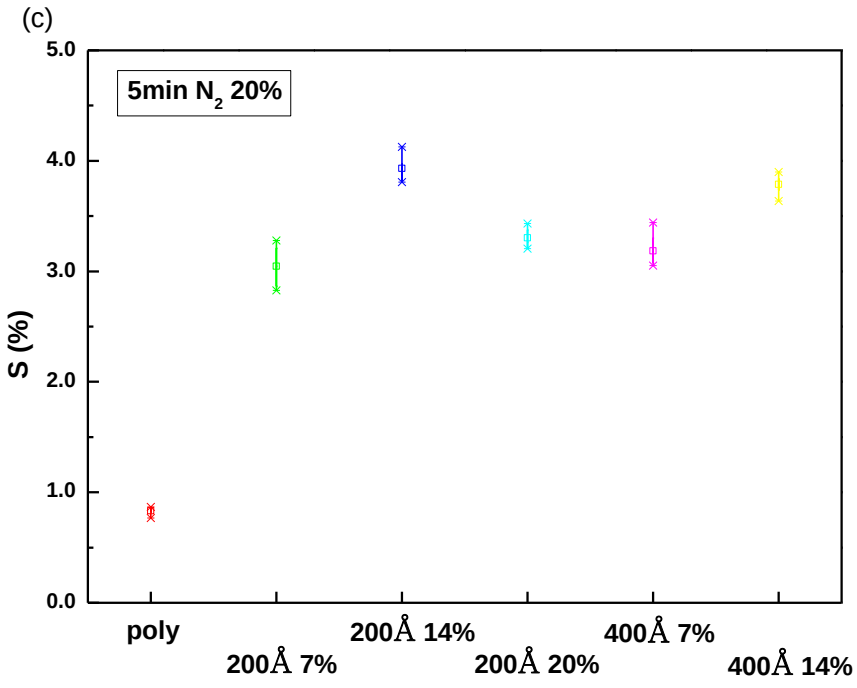

Fig.3-13 The sensitivity of different stack structure for 5min oxidation in different nitrogen/oxygen ratio, (c) the ratio of N_2 was 20%.

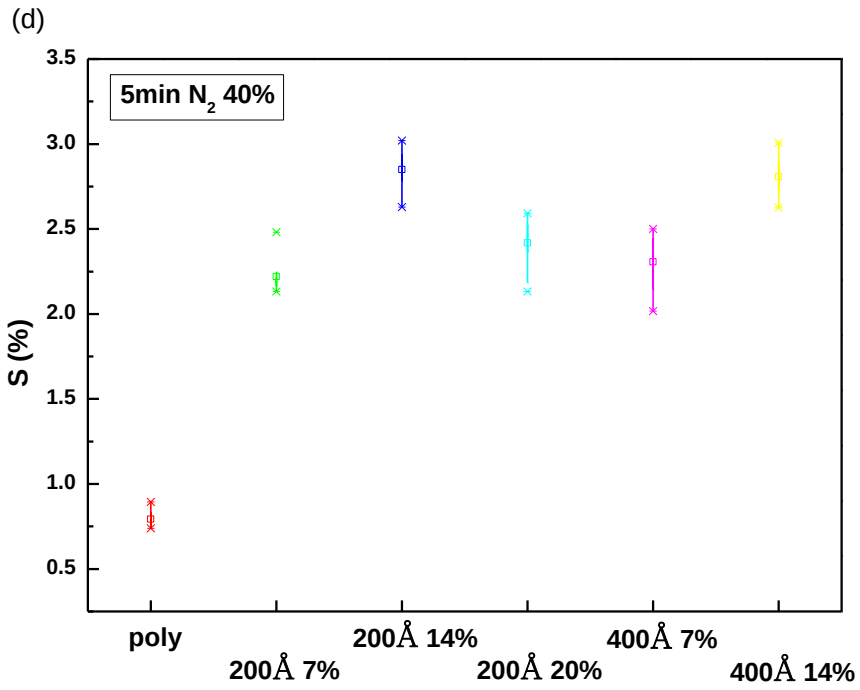

Fig.3-13 The sensitivity of different stack structure for 5min oxidation in different nitrogen/oxygen ratio, (d) the ratio of N_2 was 40%.

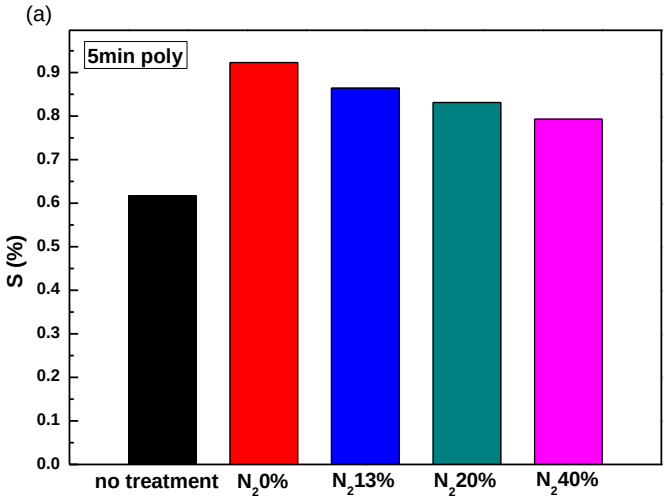

Fig.3-14 The sensitivity in varied nitrogen/oxygen ratio in different stack structure, schematic (a) is Poly-SiNW.

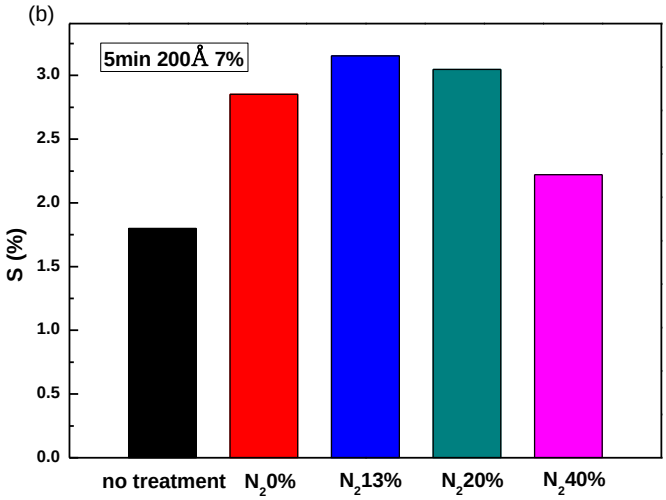

Fig.3-14 The sensitivity in varied nitrogen/oxygen ratio in different stack structure, schematic (b) is α-Si 200Å $Si_{0.93}Ge_{0.07}$.

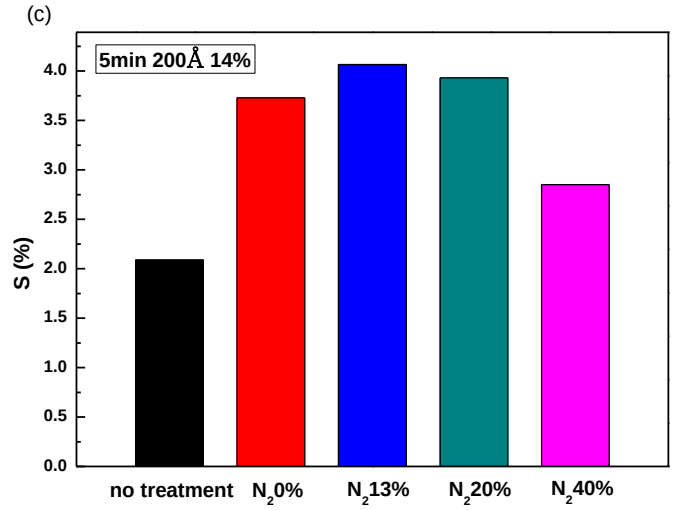

Fig.3-14 The sensitivity in varied nitrogen/oxygen ratio in different stack structure, schematic (c) is α-Si 200Å $Si_{0.86}Ge_{0.14}$.

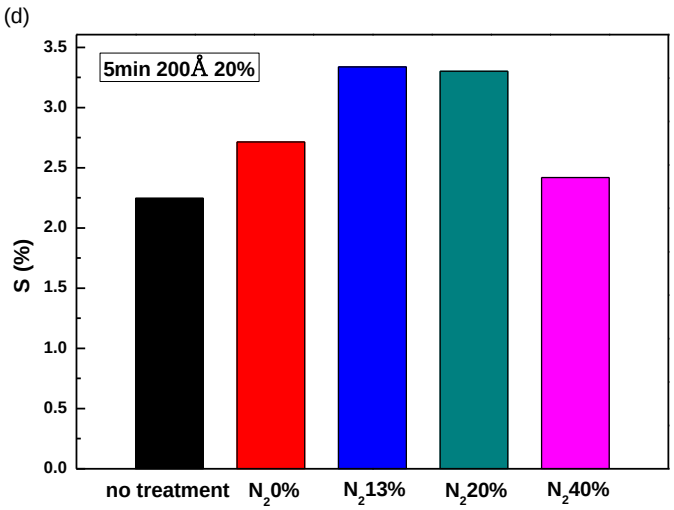

Fig.3-14 The sensitivity in varied nitrogen/oxygen ratio in different stack structure, schematic (d) is α-Si 200Å $Si_{0.80}Ge_{0.20}$.

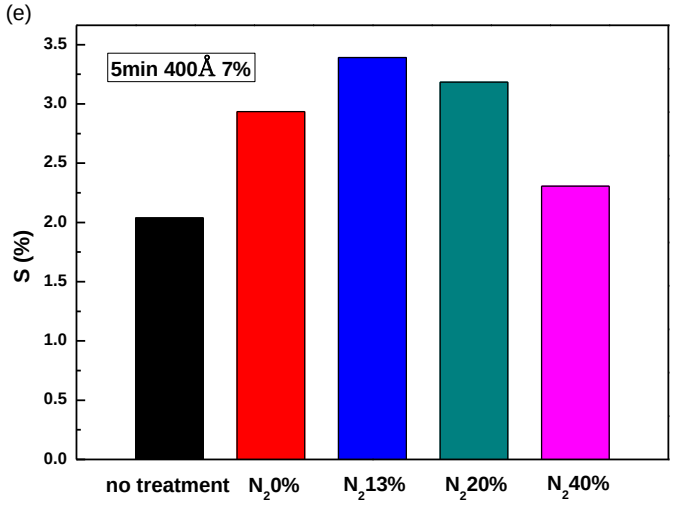

Fig.3-14 The sensitivity in varied nitrogen/oxygen ratio in different stack structure, schematic (e) is α-Si 400Å $Si_{0.93}Ge_{0.07}$.

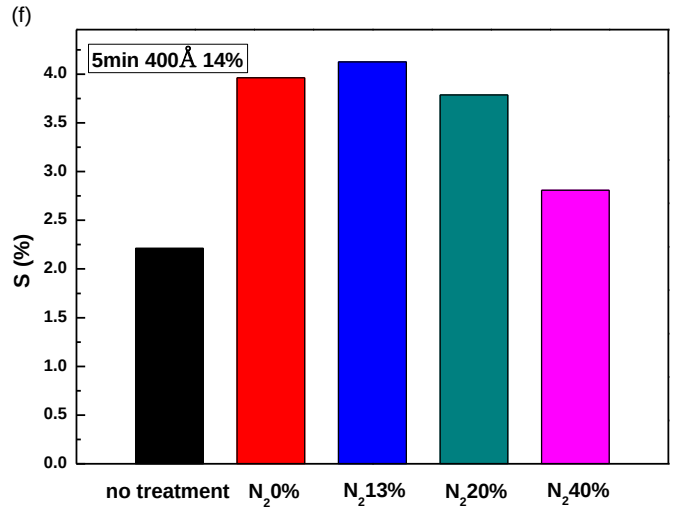

Fig.3-14 The sensitivity in varied nitrogen/oxygen ratio in different stack structure, schematic (f) is α-Si 200Å $Si_{0.86}Ge_{0.14}$.

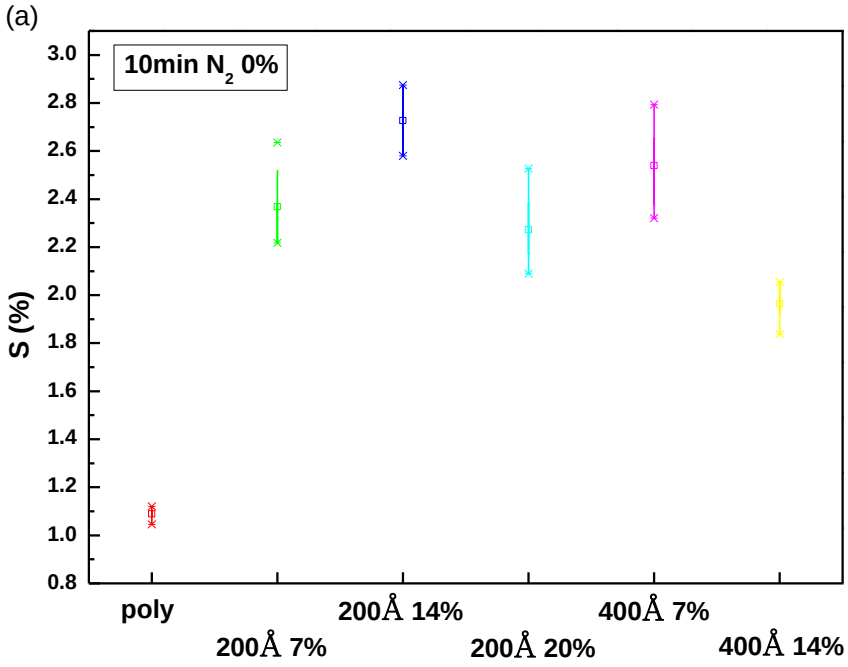

Fig.3-15 The sensitivity of different stack structure for 10min oxidation in different nitrogen/oxygen ratio, (a) the ratio of N_2 was 0%.

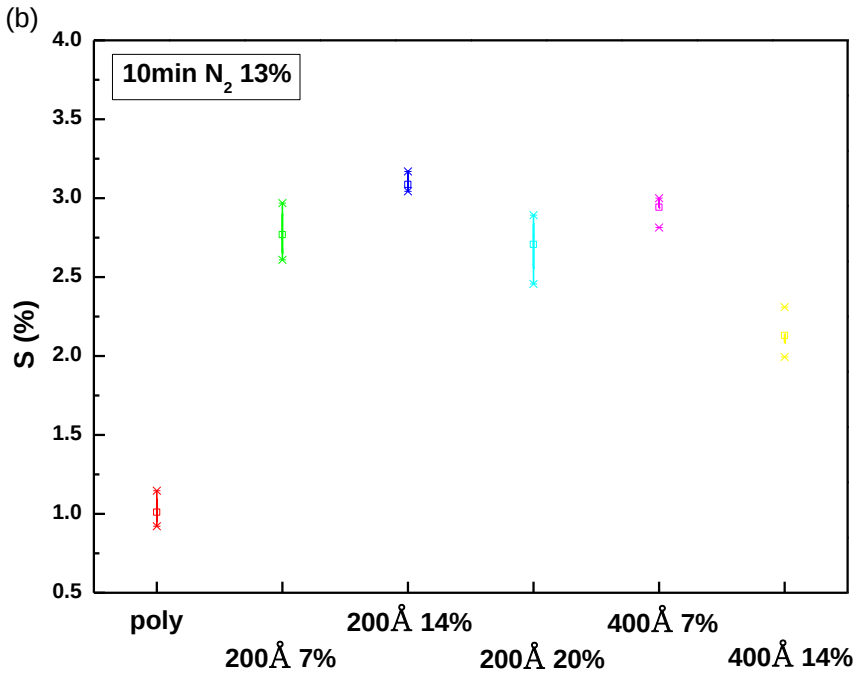

Fig.3-15 The sensitivity of different stack structure for 10min oxidation in different nitrogen/oxygen ratio, (b) the ratio of N_2 was 13%.

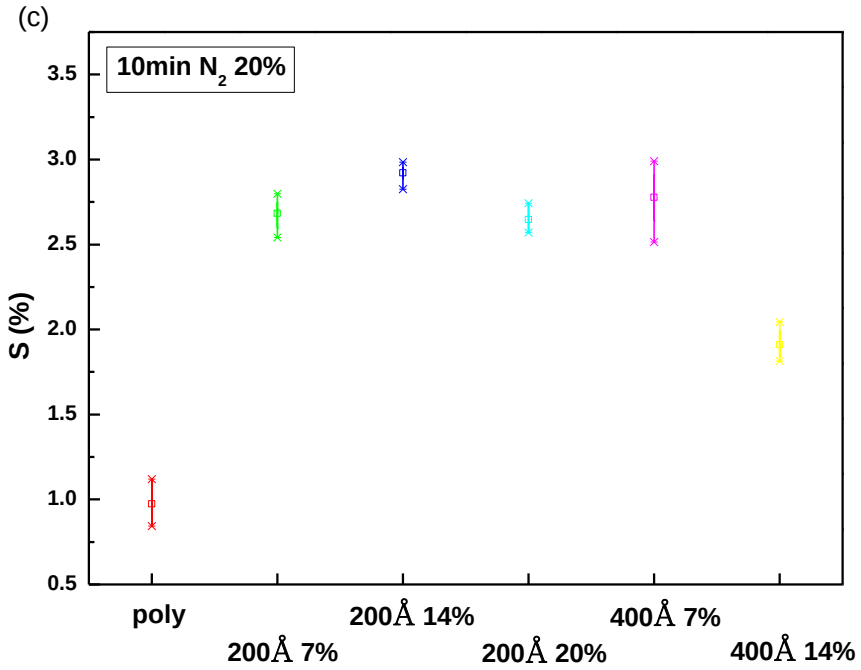

Fig.3-15 The sensitivity of different stack structure for 10min oxidation in different nitrogen/oxygen ratio, (c) the ratio of N_2 was 20%.

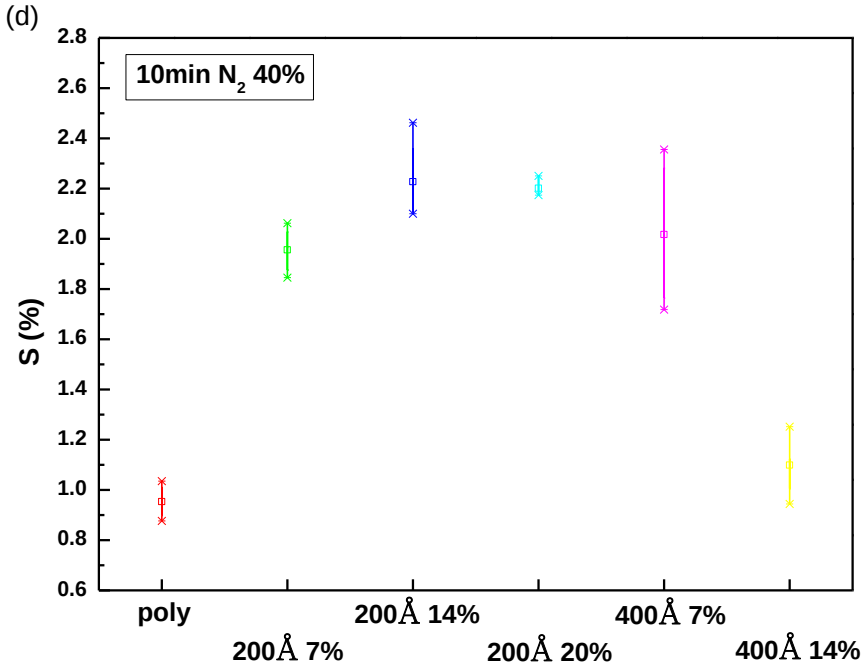

Fig.3-15 The sensitivity of different stack structure for 10min oxidation in different nitrogen/oxygen ratio, (d) the ratio of N_2 was 40%.

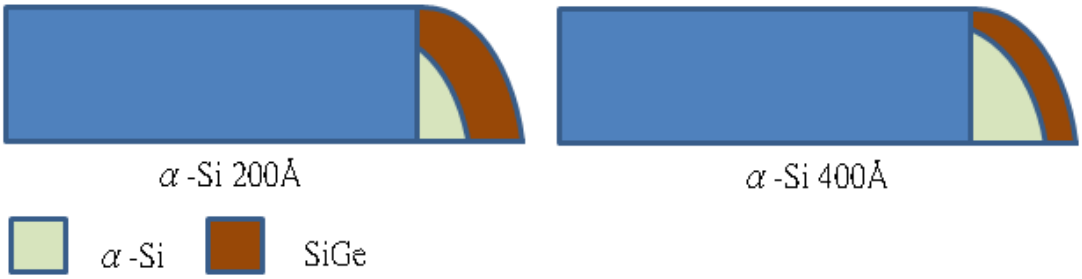

Fig.3-16 The profile of SiGeNW.

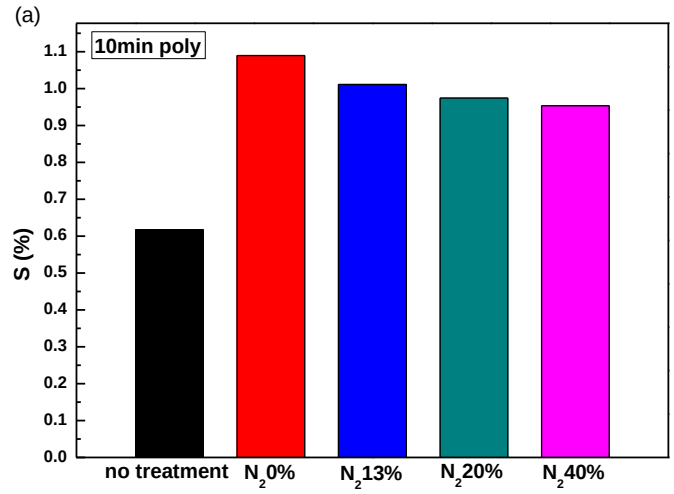

Fig.3-17 The sensitivity in varied nitrogen/oxygen ratio in different stack structure, schematic (a) is Poly-SiNW.

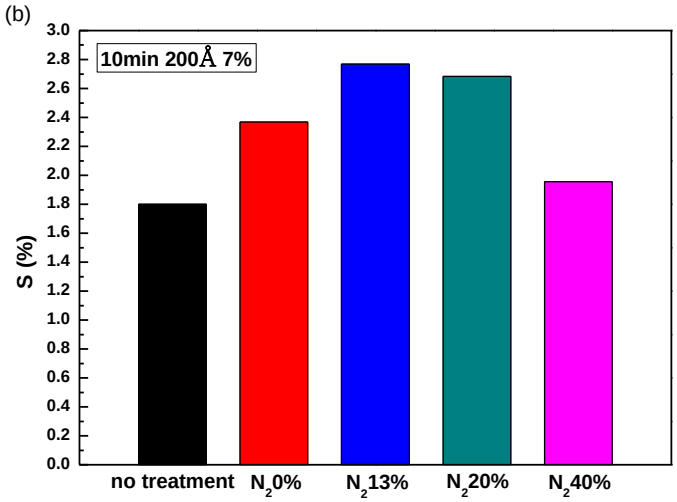

Fig.3-17 The sensitivity in varied nitrogen/oxygen ratio in different stack structure, schematic (b) is α-Si 200Å $Si_{0.93}Ge_{0.07}$.

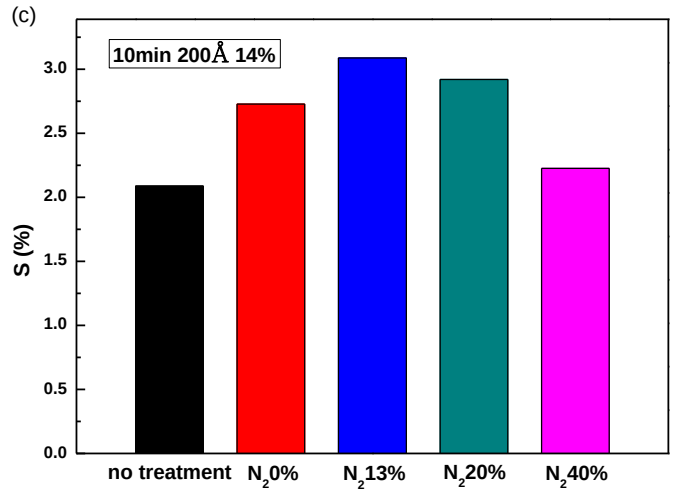

Fig.3-17 The sensitivity in varied nitrogen/oxygen ratio in different stack structure, schematic (c) is α-Si 200Å $Si_{0.86}Ge_{0.14}$.

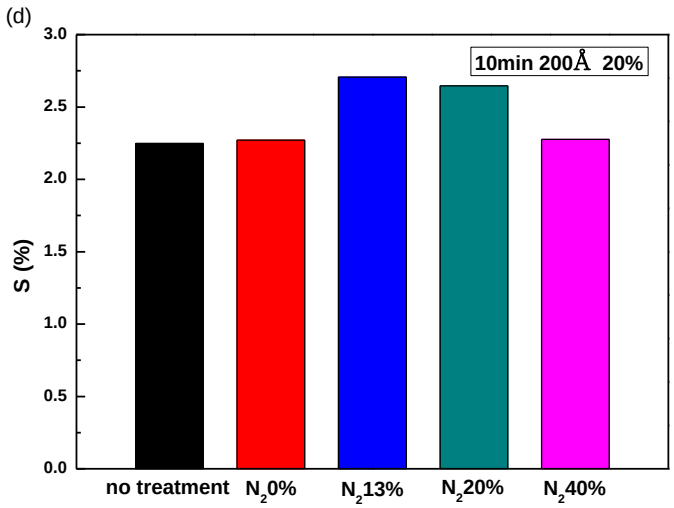

Fig.3-17 The sensitivity in varied nitrogen/oxygen ratio in different stack structure, schematic (d) is α-Si 200Å $Si_{0.80}Ge_{0.20}$.

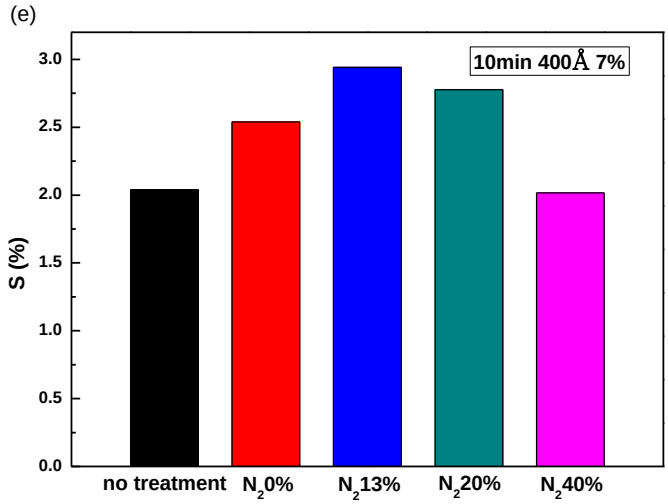

Fig.3-17 The sensitivity in varied nitrogen/oxygen ratio in different stack structure, schematic (e) is α-Si 400Å $Si_{0.93}Ge_{0.07}$.

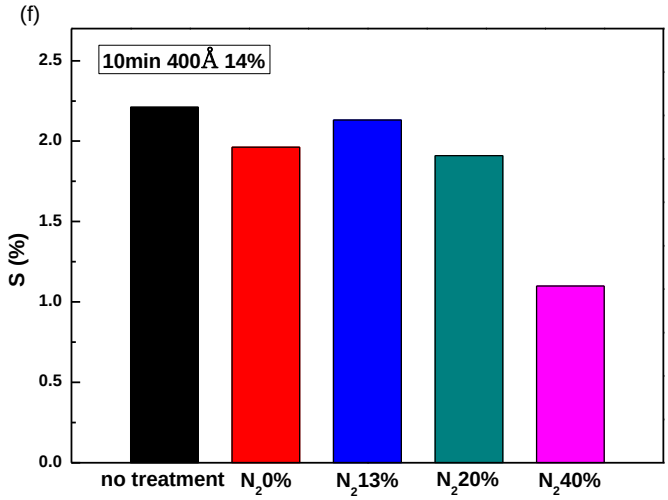

Fig.3-17 The sensitivity in varied nitrogen/oxygen ratio in different stack structure, schematic (f) is α-Si 400Å $Si_{0.86}Ge_{0.14}$.

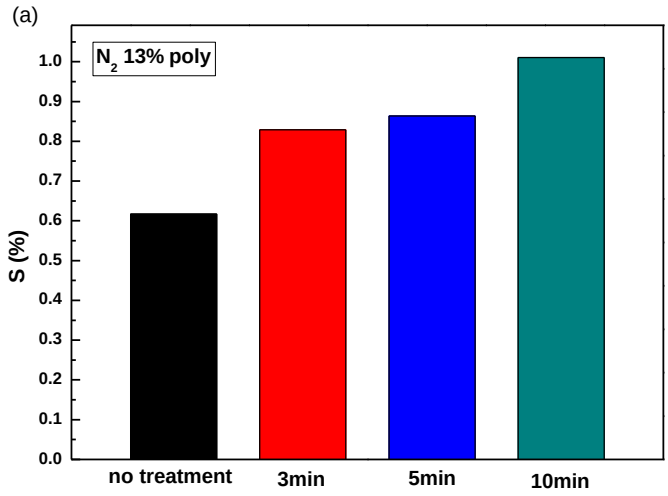

Fig.3-18 The sensitivity of N_2 13% under different stack structure (a) Poly-SiNW.

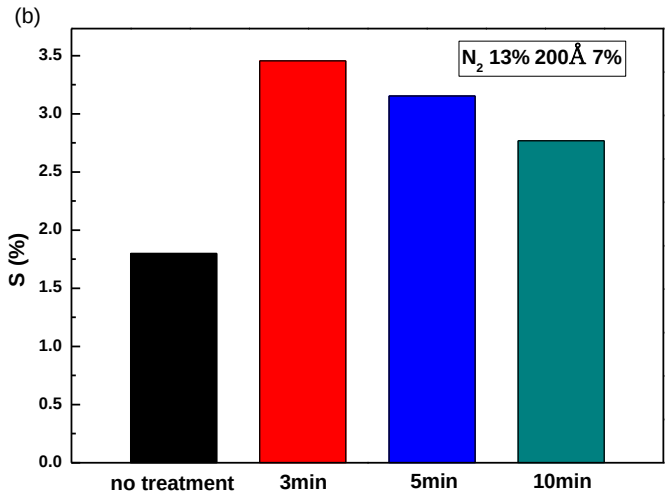

Fig.3-18 The sensitivity of N_2 13% under different stack structure (b) α-Si 200Å $Si_{0.93}Ge_{0.07}$.

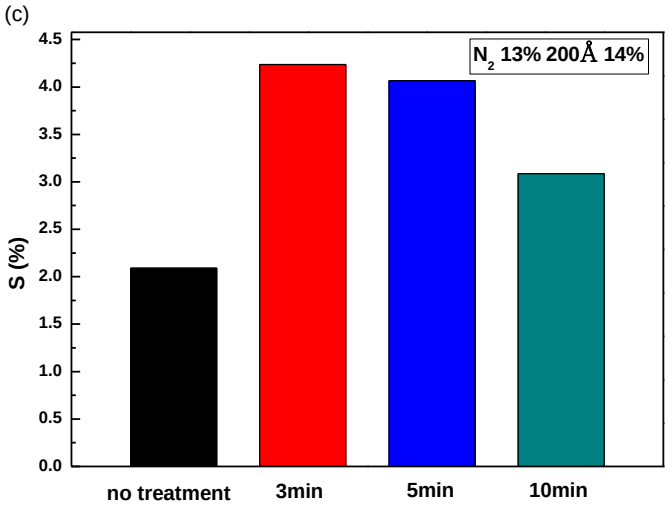

Fig.3-18 The sensitivity of N_2 13% under different stack structure (c) α-Si 200Å $Si_{0.86}Ge_{0.14}$.

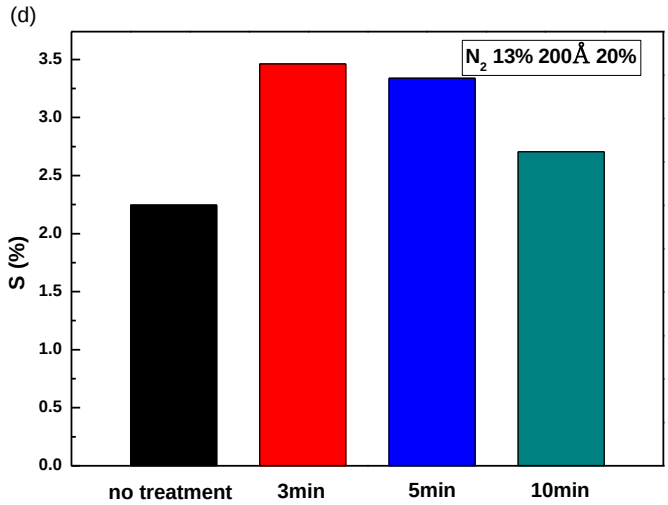

Fig.3-18 The sensitivity of N_2 13% under different stack structure (d) α-Si 200Å $Si_{0.80}Ge_{0.20}$.

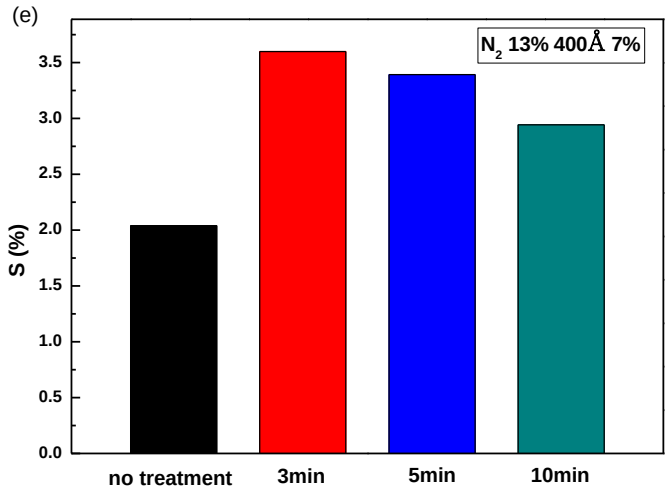

Fig.3-18 The sensitivity of N_2 13% under different stack structure (e) α-Si 400Å $Si_{0.93}Ge_{0.07}$.

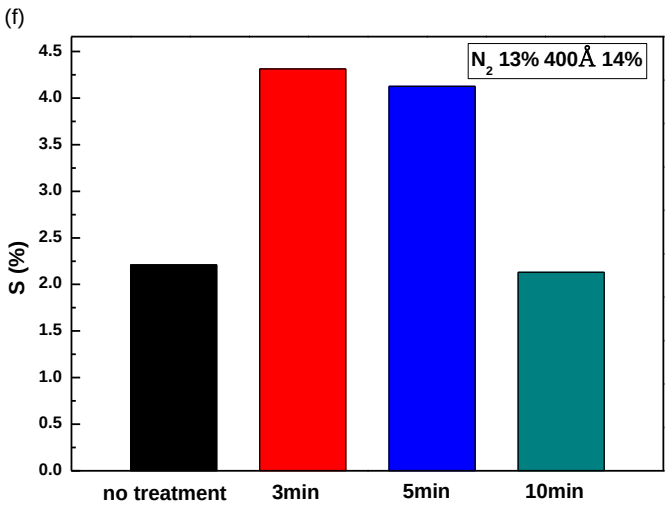

Fig.3-18 The sensitivity of N_2 13% under different stack structure (f) α-Si 400Å $Si_{0.86}Ge_{0.14}$.

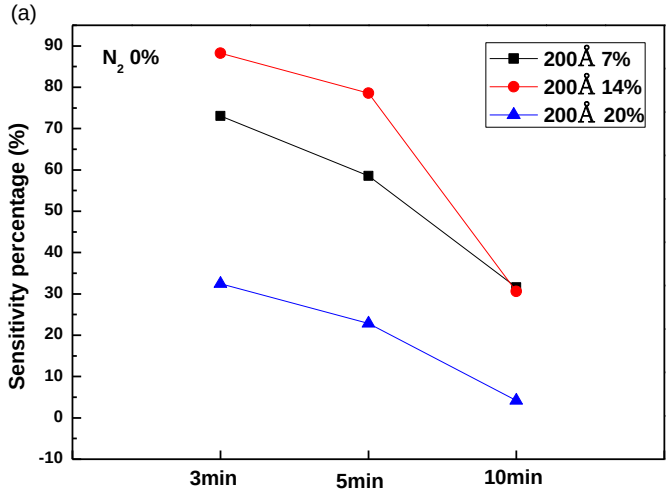

Fig.3-19 The sensitivity change percentage of α-Si 200Å in varied oxidation time for (a) N_2 0%.

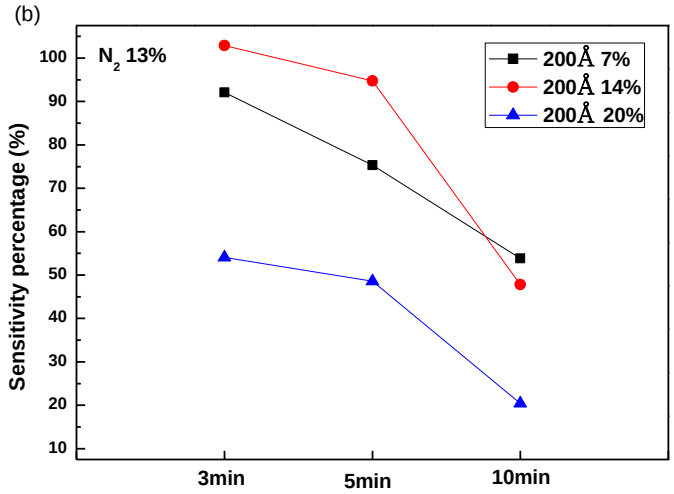

Fig.3-19 The sensitivity change percentage of α-Si 200Å in varied oxidation time for (b) N_2 13%.

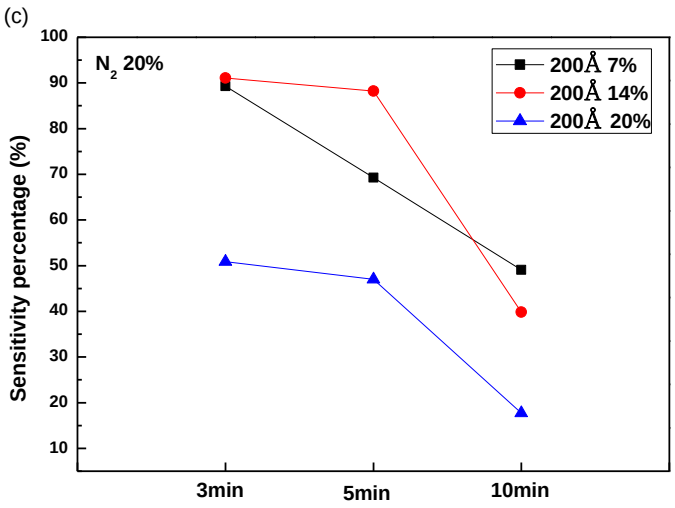

Fig.3-19 The sensitivity change percentage of α-Si 200Å in varied oxidation time for (c) N_2 20%.

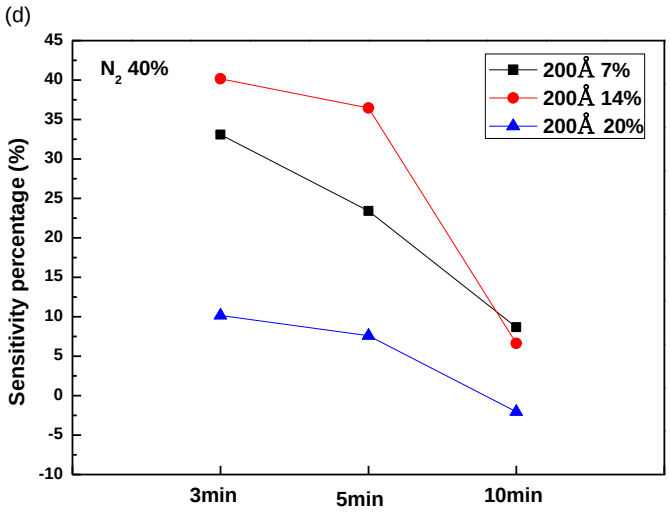

Fig.3-19 The sensitivity change percentage of α-Si 200Å in varied oxidation time for (d) N_2 40%.

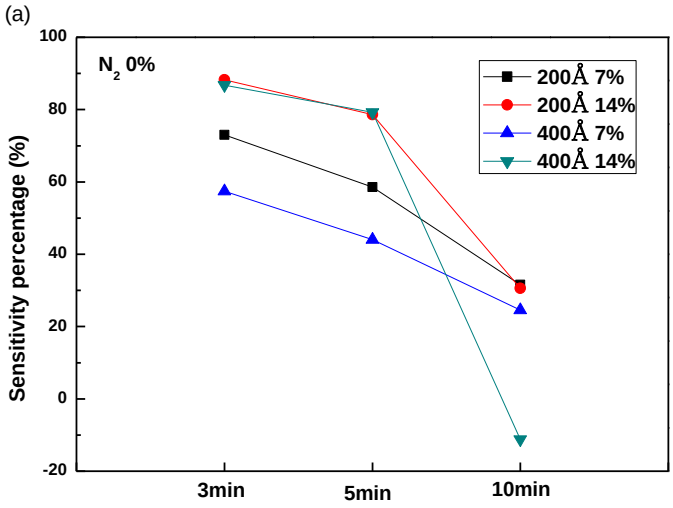

Fig.3-20 The sensitivity change percentage of α-Si 200Å and α-Si 400Å in varied oxidation time for (a) N_2 0%.

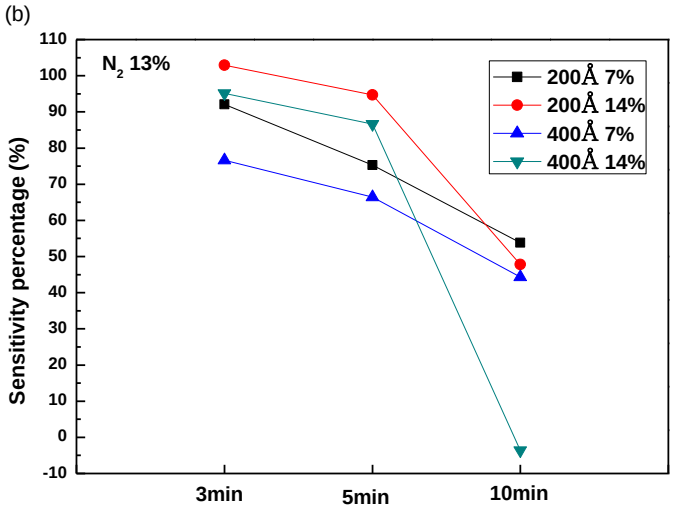

Fig.3-20 The sensitivity change percentage of α-Si 200Å and α-Si 400Å in varied oxidation time for (b) N_2 13%.

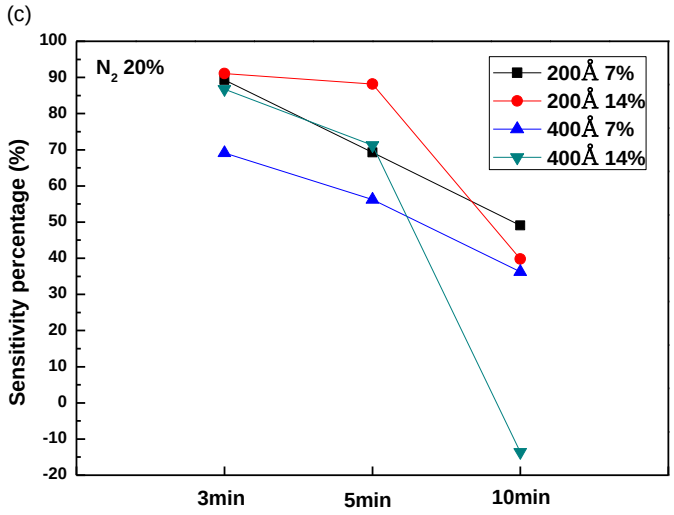

Fig.3-20 The sensitivity change percentage of α-Si 200Å and α-Si 400Å in varied oxidation time for (c) N_2 20%.

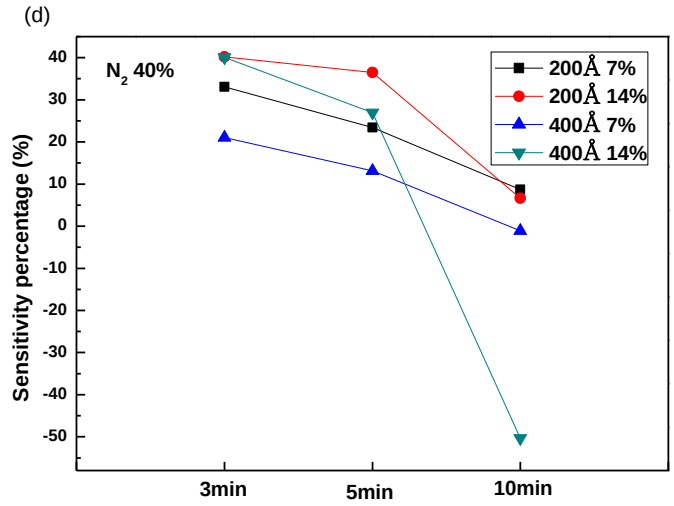

Fig.3-20 The sensitivity change percentage of α-Si 200Å and α-Si 400Å in varied oxidation time for (d) N_2 40%.

Reference

[1] P. Bergveld, “Development, Operation, and Application of the Ion-Sensitive Field-Effect Transistor as a Tool for Electrophysiology” IEEE Trans. Biomed. Eng. BME-19, 342 (1972).

[2] G. F. Blackburn, in Biosensors: Fundamentals and Applications, A. P. F. Turner, I. Karube, G. S. Wilson, Eds. (Oxford Univ. Press, Oxford, 1987), pp. 481-530.

[3] Yi Cui, Qingqiao Wei, Hongkun Park, Charles M.Lieber, “Nanowire Nanosensors for Highly Sensitive and Selective Detection of Biological and Chemical Species” SCIENCE VOL 293 17 AUGUST 2001.

[4] Y. Huang and C. M. Lieber, “Integrated nanoscale electronics and optoelectronics: Exploring nanoscale science and technology through semiconductor nanowires,” *Pure Appl. Chem.*, vol. 76, no. 12, pp. 2051–2068, Dec. 2004.

[5] M. Law, J. Goldberger, and P. Yang, “Semiconductor nanowires and nanotubes,” *Annu. Rev. Mater. Res.*, vol. 34, pp. 83–122, Aug. 2004.

[6] G. Li, N. Xi, H. Chen, A. Saeed, and M. Yu, “Assembly of nanostructure using AFM based nanomanipulation system,” in *Proc. IEEE Int. Conf. Robot. Autom.*, vol. 1, pp. 428–433, 2004.

[7] W. W. Fang, N. Singh, L. K. Bera, H. S. Nguyen, S. C. Rustagi, G. Q. Lo, N. Balasubramanian, and D.-L. Kwong, “Vertically Stacked

SiGe Nanowire Array Channel CMOS Transistors," *IEEE electron device letters*, vol. 28, no. 3, pp. 211-213, 2007.

[8] Y. F. Zhang, Y. H. Tang, N. Wang et al., "One-dimensional growth mechanism of crystalline silicon nanowires," Journal of Crystal Growth,vol. 197, no. 1-2, pp.136-140, 1999.

[9] W. S. Shi, H. Y. Peng, Y. F. Zheng et al., "Synthesis of Large Areas of Highly Oriented,Very Long Silicon Nanowires," Advanced Materials, vol. 12, no. 18, pp. 1343-1345, 2000.

[10] H. Y. Peng, Z. W. Pan, L. Xu et al., "Temperature Dependence of Si Nanowire Morphology," Advanced Materials, vol. 13, no. 5, pp. 317-320, 2001.

[11] Y. F. Zhang, Y. H. Tang, N. Wang et al., "Silicon nanowires prepared by laser ablation at high temperature," Applied Physics Letters, vol. 72, no. 15, pp. 1835-1837, 1998.

[12] N. Wang, Y. F. Zhang, Y. H. Tang et al., "SiO2-enhanced synthesis of Si nanowires by laser ablation," Applied Physics Letters, vol. 73, no. 26, pp. 3902-3904, 1998.

[13] E . S. Greiner, J. A. Gutowski, and W. C. Ellis, "Backward Waves in Longitudinally Magnetized Ferrite Rods" *J. Appl. Phys.* 32, 2489, 1961.

[14] F. C. Frank, "One-Dimensional Dislocations" *Discussions Faraday Soc.* 5, 48, 1949.

[15] R. S. Wagner and W. C. Ellis, "Vapor-Liquid-Solid Mechanism Of Single Crystal Growth" Appl. Phys. Lett. **4**, 89, 1964.

[16] A. A. Talin, L. H. Luke, L. Francois et al., "Large area, dense

silicon nanowire array chemical sensors," Applied Physics Letters, vol. 89, no. 15, pp. 153102, 2006.

[17] K. Asano, Y.-K. Choi, T.-J. King, and C. Hu, "Patterning sub-30-nm MOSFET gate with I-line lithography," *IEEE Trans. Electron Devices*,vol. 48, pp. 1004–1006, May 2001.

[18] Yang-Kyu Choi, Tsu-Jae King and Chenming Hu, "A Spacer Patterning Technology for Nanoscale CMOS" IEEE Transactions on electron devices, VOL. 49, NO. 3, MARCH 2002.

[19] R. Juhasz, N. Elfstrom, and J. Linnros, "Controlled Fabrication of Silicon Nanowires by Electron Beam Lithography and Electrochemical Size Reduction," Nano Letters, vol. 5, no. 2, pp. 275-280, 2005.

[20] E. Stern, J. F. Klemic, D. A. Routenberg et al., "Label-free immunodetection with CMOS-compatible semiconducting nanowires," Nature, vol. 445, no. 7127, pp.519-522, Feb, 2007.

[21] Y. K. Choi, N. Lindert, P. Xuan, S. Tang, D. Ha, E. Anderson, T. J. King, J. Bokor, and C. Hu, "Sub-20 nm CMOS FinFET technologies," in *IEDM Tech. Dig.*, pp. 421–424, 2001.

[22] Kook-Nyung Lee, Suk-Won Jung, Won-Hyo Kim, Min-Ho Lee, and Woo-Kyeong Seong, "Fabrication of Silicon Nanowire for Biosensor Applications," IEEE SENSORS 2006, EXCO, Daegu, Korea / October 22-25, 2006.

[23] Jong-in Hahm and Charles M. Lieber, "Direct Ultrasensitive Electrical Detection of DNA and DNA Sequence Variations Using Nanowire Nanosensors," NANO LETTERS Vol. 4, No. 1, pp.

51-54, 2004.

[24] Z. Li, Y. Chen, X. Li, T. I. Kamins, K. Nauka, and R. S. Williams, “Sequence-Specific Label-Free DNA Sensors Based on Silicon Nanowires,” Nano Letters, 4 (2), pp. 245–247, 2004.

[25] Z. Gao, A. Agarwal, A. D. Trigg et al., “Silicon Nanowire Arrays for Label-Free Detection of DNA,” Analytical Chemistry, vol. 79, no. 9, pp. 3291-3297, 2007.

[26] G. Zheng, F. Patolsky, Y. Cui et al., “Multiplexed electrical detection of cancer markers with nanowire sensor arrays,” Nat Biotech, vol. 23, no. 10, pp. 1294-1301, 2005.

[27] Fernando Patolsky, Gengfeng Zheng, Oliver Hayden, Melike Lakadamyali, Xiaowei Zhuang, and Charles M. Lieber, “Electrical detection of single viruses,” PNAS, vol. 101 no. 39 14017–14022, September 28, 2004.

[28] Jin, S., Whang, D. M., McAlpine, M. C., Friedman, R. S., Wu, Y. & Lieber, C. M, “Scalable Interconnection and Integration of Nanowire Devices without Registration,” Nano Lett. 4, pp. 915–919, 2004.

[29] Jing Wan, Shao-Ren Deng, Yifang Chen, Ejaz Huq, Ran Liu, Xin-Ping Qu, "Trilayer nanoimprint fabrication and simulation of the silicon nanowire sensor for gas detection," 2009 4th IEEE 77 International Conference on Nano/Micro Engineered and Molecular Systems, pp. 1013-1016, 2009.

[30] M. L. Y. Liu, “Growth of Aligned Square-Shaped SnO_2 Tube Arrays,” Advanced Functional Materials, vol. 15, no. 1, pp. 57-62,

2005.

[31] J. Liu, X. Wang, Q. Peng et al., “Vanadium Pentoxide Nanobelts: Highly Selective and Stable Ethanol Sensor Materials,” Advanced Materials, vol. 17, no. 6, pp. 764-767, 2005.

[32] M. A.-H. Safaa, R. T. Al-Mofarji, P. Klason et al., “Zinc oxide nanorods grown on two-dimensional macroporous periodic structures and plane Si as a pH sensor,”ournal of Applied Physics,vol. 103, no. 1, pp. 014302, 2008.

[33] X. Gou, G. Wang, J. Yang et al., “Chemical synthesis, characterisation and gas sensing performance of copper oxide nanoribbons,” Journal of Materials Chemistry, vol. 18,pp. 5, 2008.

[34] A. Kolmakov, Y. Zhang, G. Cheng, and M. Moskovits, “Detection of CO andO2 Using Tin Oxide Nanowire Sensors,” Adv. Mater, 15, No. 12 June 17, 2003.

[35] Y. Zhang, A. Kolmakov, S. Chretien et al., “Control of Catalytic Reactions at the Surface of a Metal Oxide Nanowire by Manipulating Electron Density Inside It,”Nano Letters, vol. 4, no. 3, pp. 403-407, 2004.

[36] Y. Zhang, A. Kolmakov, Y. Lilach, and M. Moskovits, “Electronic Control of Chemistry and Catalysis at the Surface of an Individual Tin Oxide Nanowire,” *J. Phys. Chem. B*, *109*, 1923-1929, 2005.

[37] L. Chao, Z. Daihua, L. Xiaolei et al., “In2O3 nanowires as chemical sensors,” Applied Physics Letters, vol. 82, no. 10, pp. 1613-1615, 2003.

[38] D. Zhang, Z. Liu, C. Li et al., “Detection of NO2 down to ppb

Levels Using Individual and Multiple In2O3 Nanowire Devices," Nano Letters, vol. 4, no. 10, pp.1919-1924, 2004.

[39] C. L. Chien, L. Sun, M. Tanase et al., "Electrodeposited magnetic nanowires: arrays,field-induced assembly, and surface functionalization," Journal of Magnetism and Magnetic Materials, vol. 249, no. 1-2, pp. 146-155, 2002.

[40] A. S. Peter, D. N. Christopher, N. J. Thomas et al., "Electric-field assisted assembly and alignment of metallic nanowires," Applied Physics Letters, vol. 77, no. 9, pp.1399-1401, 2000.

[41] F. Favier, E. C. Walter, M. P. Zach et al., "Hydrogen Sensors and Switches from Electrodeposited Palladium Mesowire Arrays," Science, vol. 293, no. 5538, pp.2227-2231, September 21, 2001.

[42] C. Z. Li, H. X. He, A. Bogozi et al., "Molecular detection based on conductance quantization of nanowires," Applied Physics Letters, vol. 76, no. 10, pp. 1333-1335, 2000.

[43] X. Wang, and C. S. Ozkan, "Multisegment nanowire sensors for the detection of DNA molecules," Nano Letters, vol. 8, no. 2, pp. 398-404, Feb, 2008.

[44] Z. Li, B. Rajendran, T. I. Kamins et al., "Silicon nanowires for sequence-specific DNA sensing: device fabrication and simulation," Applied Physics a-Materials Science & Processing, vol. 80, no. 6, pp. 1257-1263, Mar, 2005.

[45] Y. Kun, W. Hui, Z. Kai et al., "Gold nanoparticle modified silicon nanowires as biosensors," Nanotechnology, no. 11, pp. S276, 2006.

[46] P. R. Nair, and M. A. Alam, "Design considerations of silicon

nanowire biosensors,"IEEE TRANSACTIONS ON ELECTRON DEVICES, vol. 54, no. 12, pp. 3400-3408,Dec, 2007.

[47] F. K. LeGoues, R. Rosenberg, T. Nguyen et al., "Oxidation studies of SiGe," Journal of Applied Physics, vol. 65, no. 4, pp. 1724-1728, 1989.

[48] H. K. Liou, P. Mei, U. Gennser et al., "Effects of Ge concentration on SiGe oxidation behavior," Applied Physics Letters, vol. 59, no. 10, pp. 1200-1202, 1991.

[49] P. E. Hellberg, S. L. Zhang, F. M. d'Heurle et al., "Oxidation of silicon--germanium alloys. II. A mathematical model," Journal of Applied Physics, vol. 82, no. 11, pp.5779-5787, 1997.

[50] S. Balakumar, T. Jun wei1, C. H. Tung, Lo. G. Q, H. S. Nguyen, C. S. Fong, A. Agarwal R. Kumar, N. Balasubramanian, Lee. S J, and D.L. Kwong, "Fabrication of high Ge content SiGe layer on Si by Ge condensation technique," IEEE, pp. 301-305, 2006.

[51] Yong Zhang, Cheng Li,a_ Kunhuang Cai, Yanghua Chen, Songyan Chen, Hongkai Lai, and Junyong Kang, "Experimental evidence of oxidant-diffusion-limited oxidation of SiGe alloys," JOURNAL OF APPLIED PHYSICS **106**, 063508 (2009)

[52] Y. Huang, X. Duan, Q. Wei, and C.M. Lieber, "Directed Assembly of One-Dimensional Nanostructures into Functional Networks," Science 291, 630-633 (2001).

[53] X. Duan, Y. Huang, Y. Cui, J. Wang, and C.M. Lieber, "Indium phosphide nanowires as building blocks for nanoscale electronic and optoelectronic devices," Nature 409, 66-69 (2001).